

# Decoupled Divergence-Free Neural Networks Basis Method for Incompressible Fluid Problems

Jinbao Cheng <sup>\*1</sup>, Jianguo Huang <sup>†1</sup>, Haoqin Wang <sup>‡2,3</sup>, and Tao Zhou<sup>3</sup>

<sup>1</sup>School of Mathematical Sciences and MOE-LSC, Shanghai Jiao Tong University, Shanghai 200240, China

<sup>2</sup>School of Mathematics and Statistics, Yunnan University, Kunming 650500, China

<sup>3</sup>Institute of Computational Mathematics and Scientific/Engineering Computing, Academy of Mathematics and Systems Science, Chinese Academy of Sciences, Beijing 100190, China  
 Emails: jinbao\_cheng@163.com (J. Cheng), jghuang@sjtu.edu.cn (J. Huang), wanghaoqin@ynu.edu.cn (H. Wang), tzhou@lsec.cc.ac.cn (T. Zhou)

## Abstract

We propose a decoupled divergence-free neural networks basis (Decoupled-DFNN) method for solving incompressible flow problems, including the Stokes and Navier-Stokes equations. To ensure the divergence free property exactly, the velocity field is represented as the curl of a stream function in two dimensions and as the curl of a vector potential in three dimensions. Beyond classical stream-function or velocity-vorticity formulations, we further utilize the properties of the curl operator to derive two specific decoupled subproblems for the velocity (through the stream function or vector potential) and the pressure, respectively. The proposed formulations enable a sequential solution strategy, in which the velocity and pressure are solved independently. To resolve the inherent nonlinearity of the Navier-Stokes equations, we employ a Gauss-Newton linearization strategy, transforming the nonlinear velocity subproblem into a sequence of linear subproblems. These decoupled subproblems for velocity and pressure are subsequently solved using the TransNet framework. Compared with existing methods, the proposed approach reduces computational cost while strictly preserving the incompressibility constraint.

**Keywords.** extreme learning machine, decouple, divergence-free, Stokes equations, Navier-Stokes equations

**AMS subject classifications:** 65N99, 68T07

## 1 Introduction

Incompressible fluid problems have broad applications in science and engineering. However, except for a few special cases, it is impossible to get analytical solutions to these problems. To address these challenges, several classical numerical methods have been developed, including finite difference, finite element, and spectral methods [7, 26, 48, 49, 54]. In this work, we focus

---

\*This author is now working in Banma Network Technology Co., Ltd., Shanghai 200030, China

†Corresponding author

‡The work of this author was partially carried out at the Academy of Mathematics and Systems Science, Chinese Academy of Sciences

on a neural network-based numerical approach for solving the steady Stokes problem

$$\begin{cases} -\nu\Delta\mathbf{u} + \nabla p = \mathbf{f} & \text{in } \Omega, \\ \operatorname{div} \mathbf{u} = 0 & \text{in } \Omega, \\ \mathbf{u} = \mathbf{0} & \text{on } \Gamma; \end{cases} \quad \begin{array}{l} (1.1a) \\ (1.1b) \\ (1.1c) \end{array}$$

and the Navier-Stokes problem

$$\begin{cases} -\nu\Delta\mathbf{u} + (\mathbf{u} \cdot \nabla)\mathbf{u} + \nabla p = \mathbf{f} & \text{in } \Omega, \\ \operatorname{div} \mathbf{u} = 0 & \text{in } \Omega, \\ \mathbf{u} = \mathbf{0} & \text{on } \Gamma. \end{cases} \quad \begin{array}{l} (1.2a) \\ (1.2b) \\ (1.2c) \end{array}$$

Here,  $\Omega$  is a bounded simply-connected domain with Lipschitz boundary  $\Gamma$  in  $\mathbb{R}^d$  ( $d = 2, 3$ ),  $\mathbf{u}$  is the non-dimensional velocity vector,  $p$  is the non-dimensional pressure, the parameter  $\nu = R_e^{-1}$  represents the kinematic viscosity with  $R_e$  being the Reynolds number.

In recent years, machine learning techniques have been widely adopted in computational and applied mathematics, leading to the development of several neural network-based numerical methods for partial differential equations (PDEs). These approaches can be generally divided into two categories. The first category involves stochastic methods, where PDEs are reformulated as stochastic differential equations (SDEs) and solved using deep learning techniques, such as DeepBSDE [22], deep backward schemes [34], and martingale neural networks [4, 5], among others. The second category is direct methods. The most well-known of these is the physics-informed neural network (PINN) method [50]. A comprehensive review of PINN and its variants can be found in [12, 36, 43], and numerical analysis can be found in [14]. While PINNs typically aim to obtain classical solutions to PDEs, other methods have been developed to find weak solutions, such as the deep Ritz method [25], weak adversarial networks [56], and Friedrichs learning [9]. In these approaches, deep neural networks are utilized to parameterize the solutions to either SDEs or PDEs, where the network parameters are optimized to satisfy the governing physical laws. The great success of these methods is largely due to the universal approximation properties of neural networks [15, 30], particularly their ability to mitigate the ‘‘curse of dimensionality’’ [2]. For a more detailed overview of machine learning in computational mathematics, we refer the reader to [21, 23].

Although these methods have achieved significant success in various PDEs, their computational cost remains substantial, primarily due to the expensive non-convex optimization required for deep architectures. Consequently, one is tempted to utilize shallow neural networks as a solution ansatz to balance computational accuracy and efficiency. Specifically, the weights and biases of the hidden layer are randomly initialized and kept fixed, while the trainable parameters are limited to the weight coefficients of the output layer. By constructing the loss function based on the physics-informed residual minimization principle, a least-squares minimization problem with respect to the output layer weights is formed, which can be efficiently solved using existing linear or nonlinear least-squares solvers. In this way, the training process is transformed into a numerical linear algebra problem, which significantly reduce training time while preserving the approximation power of neural networks. This approach is known as the extreme learning machine (ELM) [31], with early works including [6, 20, 52]. Subsequently, Dong and Li combined non-overlapping domain decomposition with local ELM to solve PDEs [16]. In [10], the partition of unity method was combined with randomized neural networks to produce the random feature method, and [51, 53] integrated traditional numerical schemes with randomized neural networks to develop new frameworks. Furthermore, [55] adopted adaptive strategies to design an efficient algorithm. A key issue in ELM and its variants is the choice of hyperparameters. Some efficient algorithms to address this have been proposed in [17, 18]. Furthermore, [58] introduced

a strategy for generating uniformly distributed neurons in the unit ball. To unify the previous methods, Huang and Wu propose the neural network basis method and its Gauss-Newton optimizer for solving general PDEs [32]. More recently, the work was extended to handle low regularity problems [33].

In the context of fluid simulations, a number of specialized machine learning methods have also been proposed. The Stokes problem is reformulated in a first-order velocity-pressure-vorticity form, and convergence and error estimates are established for the two-dimensional case in [42]. [35] applied PINNs to solve the Navier-Stokes equations in both velocity-pressure and vorticity-velocity formulations. To accelerate training for the steady Navier-Stokes equations, [41] proposed four linearized iteration strategies. Margenberg et al. developed a hybrid solver by augmenting coarse-grid finite element simulations with fine-scale information provided by deep neural networks [44, 45]. In two dimensions, they further employed stream functions to construct structure-preserving algorithms [46]. In [57], the authors propose deep random vortex networks (DRVN), which represents the velocity field using a probabilistic formulation based on the Feynman-Kac formula. Cherepanov and Ertel extended this idea to an implicit DRVN that strictly enforces physical constraints in two dimensions without requiring the Biot-Savart kernel [11]. Additionally, [37] combined PINNs with PointNet to solve Navier-Stokes problems on irregular geometries. As for the error analysis, [47] derived a priori and a posteriori error estimates for the Stokes problem solved by the deep Ritz method, while [13] establishes rigorous error bounds for PINN approximations of the incompressible Navier-Stokes equations.

It is worth mentioning that the divergence-free condition is a fundamental conservation law in incompressible fluid flows, which means the mass conservation of the underlying fluid. Most existing methods enforce this constraint through adding penalty terms in the loss function, but it is a critical issue to choose the penalty parameter feasibly. The other way is to use the stream function based formulations in two dimensions (cf. [42, 46]), which can ensure the incompressibility exactly. However, it is a major challenge to extend this approach to three dimensions. Moreover, even regardless of whether a velocity-pressure or velocity-vorticity formulation is adopted (cf. [35]), the resulting system consists of coupled PDEs in which the unknown variables must be solved simultaneously, leading to high computational complexity.

In this paper, we propose the decoupled divergence-free neural networks basis (Decoupled-DFNN) method for numerically solving the steady Stokes equation and Navier-Stokes equation in two-dimensions and three-dimensions. We treat the incompressibility requirement as a linear constraint. Following the general framework for exact enforcement of linear constraints  $\mathcal{A}(u) = 0$  introduced in [19], one needs to construct a linear operator  $\mathcal{G}$  such that

$$\text{im}(\mathcal{G}) \subset \ker(\mathcal{A}),$$

By substituting the solution ansatz  $u = \mathcal{G}(v)$ , the constraint is satisfied exactly along the solution trajectory, i.e.  $\mathcal{A} \circ \mathcal{G}(v) = 0$ . In our context,  $\mathcal{A} = \text{div}$ , and we employ the theory of vector fields to construct the operator  $\mathcal{G}$  depending on the dimensionality. In the two-dimensional case, we build upon the well-established stream function formulation [48]. While traditional applications of this technique typically involve solving a system where the stream function and pressure remain coupled, we introduce a further refinement. By applying the curl operator to both sides of the governing equations, we eliminate the pressure gradient and derive a fully decoupled subproblem for the velocity field (represented by the stream function), as discussed in [28, 39]. This subproblem is then solved efficiently using the TransNet framework. Once the velocity field is obtained, the remaining governing equation reduces to a pressure-only problem, for which a classical solution can be recovered efficiently by TransNet as well. In the three-dimensional case, our method draws inspiration from the vorticity-vector potential formulations [24, 40]. Whereas standard formulations of this type often involve a coupling between the potential

and vorticity, our approach further transforms the governing equations to derive a decoupled subproblem formulated solely for the vector potential by utilizing the properties of the curl operator. This extension allows us to resolve the velocity field (represented by the vector potential) without simultaneous calculation of the vorticity or pressure. Subsequently, the pressure field is recovered from the resolved velocity. Similarly, the decoupled subproblems are resolved by the TransNet. Compared with existing methods, the Decoupled-DFNN significantly reduces computational cost by breaking these traditional couplings while strictly preserving the incompressibility constraint to machine precision. Our contributions are summarized as follows:

- We derive decoupled divergence-free formulations for incompressible flows in both two and three dimensions, leading to single-field subproblems for the velocity representation (stream function in 2D and vector potential in 3D) that are free of pressure and vorticity coupling.
- We develop a neural network-based framework to efficiently solve the resulting decoupled subproblems for both velocity and pressure. The key advantage lies in its mesh-free feature.
- We demonstrate that the proposed Decoupled-DFNN enforces the divergence-free constraint to machine precision while significantly reducing computational cost.

The rest of this paper is organized as follows. Section 2 introduces decoupled divergence free formulations for the Stokes and Navier-Stokes equations in both two and three dimensions. Based on these formulations, Decoupled-DFNN methods are proposed in Section 3. Section 4 presents several numerical experiments to demonstrate the performance of the proposed methods. Conclusions are drawn in the last section.

## 2 Preliminaries

In this section, we first recall several fundamental results on vector fields (cf. [26, 48]), and then derive identities for the nonlinear advection term that will be used in the subsequent analysis. Throughout this paper, we adopt standard notation for Sobolev spaces [1]

Let  $\Omega \subset \mathbb{R}^2$  be a bounded simply-connected domain with Lipschitz boundary. For  $\psi \in \mathcal{D}'(\Omega)$  and  $\mathbf{v} = [v_1, v_2]^T \in [\mathcal{D}'(\Omega)]^2$ , define

$$\mathbf{curl} \psi := \left[ \frac{\partial \psi}{\partial y}, -\frac{\partial \psi}{\partial x} \right]^T, \quad \mathbf{curl} \mathbf{v} := \frac{\partial v_2}{\partial x} - \frac{\partial v_1}{\partial y}.$$

**Lemma 2.1** (Theorem 3.1 in [26]). A function  $\mathbf{v} \in [L^2(\Omega)]^2$  satisfies

$$\operatorname{div} \mathbf{v} = 0, \quad \text{and} \quad \int_{\partial\Omega} \mathbf{v} \cdot \mathbf{n} \, ds = 0,$$

if and only if there exists a stream function  $\psi \in H^1(\Omega)$  such that

$$\mathbf{v} = \mathbf{curl} \psi.$$

Here and below,  $\mathbf{n}$  indicates the unit outward normal vector on the boundary.

Let  $\Omega \subset \mathbb{R}^3$  be a bounded simply-connected region with Lipschitz boundary. Define the curl operator for distribution  $\mathbf{v} = [v_1, v_2, v_3]^T \in [\mathcal{D}'(\Omega)]^3$  by

$$\mathbf{curl} \mathbf{v} := \nabla \times \mathbf{v} = \left[ \frac{\partial v_3}{\partial y} - \frac{\partial v_2}{\partial z}, \frac{\partial v_1}{\partial z} - \frac{\partial v_3}{\partial x}, \frac{\partial v_2}{\partial x} - \frac{\partial v_1}{\partial y} \right]^T.$$

**Lemma 2.2** (Theorems 3.4 and 3.5 in [26]). A vector field  $\mathbf{v} \in [L^2(\Omega)]^3$  satisfies

$$\operatorname{div} \mathbf{v} = 0, \text{ and } \int_{\partial\Omega} \mathbf{v} \cdot \mathbf{n} \, ds = 0,$$

if and only if there exists a potential function  $\boldsymbol{\psi} \in [H^1(\Omega)]^3$  such that

$$\mathbf{v} = \mathbf{curl} \boldsymbol{\psi}, \quad \operatorname{div} \boldsymbol{\psi} = 0.$$

Furthermore, we can choose  $\boldsymbol{\psi} \in H(\mathbf{curl}; \Omega)$  satisfies

$$\boldsymbol{\psi} \cdot \mathbf{n} = 0 \quad \text{on } \Gamma.$$

**Lemma 2.3** (cf. [26, 48]). For any vector function  $\mathbf{v}, \boldsymbol{\psi} \in [C^1(\Omega)]^3$ , there hold

$$(\mathbf{v} \cdot \nabla) \mathbf{v} = \frac{1}{2} \nabla |\mathbf{v}|^2 - \mathbf{v} \times (\nabla \times \mathbf{v}), \quad (2.1)$$

$$\nabla \times (\boldsymbol{\psi} \times \mathbf{v}) = (\nabla \cdot \mathbf{v}) \boldsymbol{\psi} - (\nabla \cdot \boldsymbol{\psi}) \mathbf{v} + (\mathbf{v} \cdot \nabla) \boldsymbol{\psi} - (\boldsymbol{\psi} \cdot \nabla) \mathbf{v}. \quad (2.2)$$

Moreover, if  $\mathbf{v} \in [C^2(\Omega)]^3$ , then

$$\nabla \times (\nabla \times \mathbf{v}) = \nabla(\nabla \cdot \mathbf{v}) - \Delta \mathbf{v}. \quad (2.3)$$

With the above results in mind, we can obtain the following two identities.

**Theorem 2.1.** Let  $\Omega \subset \mathbb{R}^2$  be a bounded domain with Lipschitz boundary and  $\phi \in C^3(\Omega)$  a stream function with  $\mathbf{u} = \mathbf{curl} \phi$ . Then there holds

$$\operatorname{curl}((\mathbf{u} \cdot \nabla) \mathbf{u}) = -(\mathbf{curl} \phi \cdot \nabla) \Delta \phi. \quad (2.4)$$

*Proof.* By the definition of the curl operator and the chain rule, we have

$$\begin{aligned} \operatorname{curl}((\mathbf{u} \cdot \nabla) \mathbf{u}) &= \frac{\partial}{\partial x} \left( u_1 \frac{\partial u_2}{\partial x} + u_2 \frac{\partial u_2}{\partial y} \right) - \frac{\partial}{\partial y} \left( u_1 \frac{\partial u_1}{\partial x} + u_2 \frac{\partial u_1}{\partial y} \right) \\ &= u_1 \left( \frac{\partial^2 u_2}{\partial x^2} - \frac{\partial^2 u_1}{\partial y \partial x} \right) + u_2 \left( \frac{\partial^2 u_2}{\partial x \partial y} - \frac{\partial^2 u_1}{\partial y^2} \right) + \left( \frac{\partial u_1}{\partial x} + \frac{\partial u_2}{\partial y} \right) \left( \frac{\partial u_2}{\partial x} - \frac{\partial u_1}{\partial y} \right) \\ &= u_1 \left( \frac{\partial^2 u_2}{\partial x^2} - \frac{\partial^2 u_1}{\partial x \partial y} \right) + u_2 \left( \frac{\partial^2 u_2}{\partial y \partial x} - \frac{\partial^2 u_1}{\partial y^2} \right) + \operatorname{div} \mathbf{u} \cdot \mathbf{curl} \mathbf{v}, \end{aligned}$$

which combined with  $\operatorname{div} \mathbf{u} = 0$  implies

$$\operatorname{curl}((\mathbf{u} \cdot \nabla) \mathbf{u}) = u_1 \frac{\partial}{\partial x} \left( \frac{\partial u_2}{\partial x} - \frac{\partial u_1}{\partial y} \right) + u_2 \frac{\partial}{\partial y} \left( \frac{\partial u_2}{\partial x} - \frac{\partial u_1}{\partial y} \right).$$

Finally, substituting  $\mathbf{u} = \mathbf{curl} \phi$  into above expression yields

$$\begin{aligned} \operatorname{curl}((\mathbf{u} \cdot \nabla) \mathbf{u}) &= u_1 \frac{\partial}{\partial x} \left( -\frac{\partial^2 \phi}{\partial x^2} - \frac{\partial^2 \phi}{\partial y^2} \right) + u_2 \frac{\partial}{\partial y} \left( -\frac{\partial^2 \phi}{\partial x^2} - \frac{\partial^2 \phi}{\partial y^2} \right) \\ &= -(\mathbf{u} \cdot \nabla) \Delta \phi = -(\mathbf{curl} \phi \cdot \nabla) \Delta \phi. \end{aligned}$$

□

**Theorem 2.2.** Let  $\Omega \subset \mathbb{R}^3$  be a bounded domain with Lipschitz boundary and  $\boldsymbol{\phi} \in [C^3(\Omega)]^3$  a potential vector such that  $\mathbf{u} = \mathbf{curl} \boldsymbol{\phi}$  and  $\operatorname{div} \boldsymbol{\phi} = 0$ . Then there holds

$$\operatorname{curl}((\mathbf{u} \cdot \nabla) \mathbf{u}) = (\Delta \boldsymbol{\phi} \cdot \nabla) \mathbf{curl} \boldsymbol{\phi} - (\mathbf{curl} \boldsymbol{\phi} \cdot \nabla) \Delta \boldsymbol{\phi}. \quad (2.5)$$

*Proof.* Write  $\boldsymbol{\omega} = \mathbf{curl} \mathbf{u}$ , meaning the vorticity of  $\mathbf{u}$ . By the identity (2.1),

$$\mathbf{curl}((\mathbf{u} \cdot \nabla)\mathbf{u}) = \frac{1}{2}\nabla \times (\nabla|\mathbf{u}|^2) - \nabla \times (\mathbf{u} \times (\nabla \times \mathbf{u})).$$

Noting that  $\nabla \times \nabla f = 0$  for any scale function  $f$ , we see that

$$\mathbf{curl}((\mathbf{u} \cdot \nabla)\mathbf{u}) = -\nabla \times (\mathbf{u} \times \boldsymbol{\omega}) = \nabla \times (\boldsymbol{\omega} \times \mathbf{u}), \quad (2.6)$$

which combined with (2.2) yields

$$\nabla \times (\boldsymbol{\omega} \times \mathbf{u}) = (\mathbf{u} \cdot \nabla)\boldsymbol{\omega} - (\boldsymbol{\omega} \cdot \nabla)\mathbf{u} + (\nabla \cdot \mathbf{u})\boldsymbol{\omega} - (\nabla \cdot \boldsymbol{\omega})\mathbf{u}.$$

Since  $\operatorname{div} \mathbf{u} = 0$  and  $\nabla \cdot \nabla \times \mathbf{v} = 0$  for any vector field  $\mathbf{v}$ , we can rewrite (2.6) as

$$\mathbf{curl}((\mathbf{u} \cdot \nabla)\mathbf{u}) = (\mathbf{u} \cdot \nabla)\boldsymbol{\omega} - (\boldsymbol{\omega} \cdot \nabla)\mathbf{u}. \quad (2.7)$$

Using (2.3), we obtain

$$\boldsymbol{\omega} = \mathbf{curl} \mathbf{u} = \mathbf{curl}(\mathbf{curl} \phi) = \nabla(\nabla \cdot \phi) - \Delta \phi = -\Delta \phi. \quad (2.8)$$

Substituting (2.8) into (2.7) gives

$$\mathbf{curl}((\mathbf{u} \cdot \nabla)\mathbf{u}) = -(\mathbf{u} \cdot \nabla)\Delta \phi + (\Delta \phi \cdot \nabla)\mathbf{u} = (\Delta \phi \cdot \nabla)\mathbf{curl} \phi - (\mathbf{curl} \phi \cdot \nabla)\Delta \phi.$$

□

### 3 Decoupled divergence-free formulations for incompressible flows

In this section, we derive the decoupled divergence-free formulas for the steady Stoke and the Navier-Stokes equations in  $\mathbb{R}^2$  and  $\mathbb{R}^3$ . The results in three dimensions differ from the classical vorticity-velocity (or vorticity-vector potential) formulations usually used in the literature.

#### 3.1 The 2D case: stream function representation

We first consider the two-dimensional Stokes equations (1.1a)–(1.1c). By the divergence theorem and the incompressibility constraint, it follows that

$$\int_{\Gamma} \mathbf{u} \cdot \mathbf{n} \, ds = \int_{\Omega} \operatorname{div} \mathbf{u} \, dx = 0.$$

This identity implies that for any divergence-free velocity field  $\mathbf{u} \in [H^1(\Omega)]^2$ , there exists a stream function  $\phi \in H^2(\Omega)$  such that  $\mathbf{u}$  can be represented via  $\phi$  (cf. Lemma 2.1).

To derive a decoupled, divergence-free formulation, we first reformulate the governing equations in terms of  $\phi$ . Suppose  $\mathbf{u} \in [H^3(\Omega)]^2$  and  $\phi \in H^4(\Omega)$ . Then applying the curl operator to the left-hand side of (1.1a) yields

$$\mathbf{curl}(-\nu \Delta \mathbf{curl} \phi + \nabla p) = -\nu \Delta \mathbf{curl} \mathbf{curl} \phi + \mathbf{curl} \nabla p = \nu \Delta^2 \phi.$$

Moreover, a direct computation confirms that  $\operatorname{div} \mathbf{curl} \phi = 0$ . Consequently, (1.1a)–(1.1b) can be transformed into the following decoupled biharmonic equation

$$\nu \Delta^2 \phi = \mathbf{curl} \mathbf{f} \quad \text{in } \Omega.$$

Concerning the boundary condition (1.1c), the no-slip condition  $\mathbf{u} = 0$  implies

$$\begin{cases} \mathbf{u} \cdot \mathbf{n}_0 = \operatorname{curl} \phi \cdot \mathbf{n}_0 = \nabla \phi \cdot \boldsymbol{\tau}_0 = 0, \\ \mathbf{u} \cdot \boldsymbol{\tau}_0 = \operatorname{curl} \phi \cdot \boldsymbol{\tau}_0 = -\nabla \phi \cdot \mathbf{n}_0 = 0, \end{cases}$$

where  $\mathbf{n}_0$  and  $\boldsymbol{\tau}_0$  denote the unit outward normal and unit tangent vector on  $\Gamma$ , respectively. In other words, we have

$$\nabla \phi = \mathbf{0} \quad \text{on } \Gamma. \quad (3.1)$$

From (3.1), we know  $\phi$  is constant along the boundary. Since the velocity field depends only on the derivatives of  $\phi$ , we impose  $\phi = 0$  on  $\Gamma$  without loss of generality to ensure the uniqueness of the solution. So the decoupled subproblem for the velocity in terms of  $\phi \in H_0^2(\Omega)$  reads

$$\begin{cases} \nu \Delta^2 \phi = \operatorname{curl} \mathbf{f} & \text{in } \Omega, \\ \phi = \frac{\partial \phi}{\partial n} = 0 & \text{on } \Gamma. \end{cases} \quad (3.2)$$

**Remark 3.1.** If we consider the slip condition  $\mathbf{u} = \mathbf{g}$  on the boundary  $\Gamma$ , a similar derivation gives

$$\begin{cases} \mathbf{u} \cdot \mathbf{n}_0 = \nabla \phi \cdot \boldsymbol{\tau}_0 = \mathbf{g} \cdot \mathbf{n}_0, \\ \mathbf{u} \cdot \boldsymbol{\tau}_0 = -\nabla \phi \cdot \mathbf{n}_0 = \mathbf{g} \cdot \boldsymbol{\tau}_0, \end{cases}$$

Thus, we can impose the constraint of  $\phi$  on the boundary.

Once the velocity  $\mathbf{u} = \mathbf{curl} \phi$  is determined, the pressure  $p$  can be computed from

$$\nabla p = \mathbf{f} + \nu \Delta \mathbf{u}.$$

To ensure a unique solution for the pressure, we impose an additional reference constraint

$$p(\mathbf{x}_0) = 0,$$

where  $\mathbf{x}_0$  is any given point in the interior of  $\Omega$ . Thus, the decoupled subproblem for the pressure reads

$$\begin{cases} \nabla p = \mathbf{f} + \nu \Delta \mathbf{u}, & \text{in } \Omega, \\ p(\mathbf{x}_0) = 0. \end{cases} \quad (3.3)$$

Next, we extend our framework to the steady Navier-Stokes equations (1.2a)–(1.2c). As in the Stokes case, applying the curl operator to (1.2a) eliminates the pressure term. The only additional term is the nonlinear advection term. By Theorem 2.1, its curl admits the representation (2.4). Combing (3.2) and (2.4) yields the decoupled subproblem for the velocity

$$\begin{cases} \nu \Delta^2 \phi - (\mathbf{curl} \phi \cdot \nabla) \Delta \phi = \operatorname{curl} \mathbf{f} & \text{in } \Omega, \\ \phi = \frac{\partial \phi}{\partial n} = 0 & \text{on } \Gamma. \end{cases} \quad (3.4)$$

Similarly, the decoupled subproblem for the pressure reads

$$\begin{cases} \nabla p = \mathbf{f} + \nu \Delta \mathbf{u} - (\mathbf{u} \cdot \nabla) \mathbf{u}, & \text{in } \Omega, \\ p(\mathbf{x}_0) = 0. \end{cases} \quad (3.5)$$

Although formulation (3.4) has been studied in [28, 39], and Legendre spectral methods were further developed for two-dimensional Navier-Stokes problems in [27], extending these techniques to the three-dimensional setting involves additional technical considerations and is not entirely straightforward. Moreover, (3.5) allows the recovery of a classical solution, in contrast to the weak solution frameworks commonly adopted in earlier works.

### 3.2 The 3D case: vector potential representation

It can be verified that the solution to (1.1a)–(1.1c) satisfies the assumptions of Lemma 2.2 by the divergence theorem and the incompressibility constraint. Moreover, since  $\Omega$  is a simply-connected domain, there exists a unique potential function  $\phi \in H(\mathbf{curl}; \Omega)$  such that the velocity can be represented by  $\mathbf{u} = \mathbf{curl} \phi$ . To ensure sufficient regularity for the derivation of the decoupled, divergence-free formulation, we assume that  $\mathbf{u} \in [H^3(\Omega)]^3$  and  $\phi \in [H^4(\Omega)]^3$ .

Taking the  $\mathbf{curl}$  of the left side of (1.1a) yields

$$\mathbf{curl}(-\nu\Delta \mathbf{curl} \phi + \nabla p) = -\nu\Delta \mathbf{curl} \mathbf{curl} \phi + \mathbf{curl} \nabla p = -\nu\Delta(\nabla(\nabla \cdot \phi) - \Delta\phi).$$

Noticing that  $\phi$  is divergence-free, the above expression further simplifies to

$$\nu\Delta^2\phi = \mathbf{curl} \mathbf{f}. \quad (3.6)$$

A direct computation confirms that  $\text{div} \mathbf{curl} \phi = 0$ , so the incompressibility constraint is satisfied identically. Combing (3.6), Lemma 2.2 and the boundary condition (1.2c), we obtain the following decoupled subproblem for the velocity, expressed in terms of  $\phi$

$$\begin{cases} \nu\Delta^2\phi = \mathbf{curl} \mathbf{f} & \text{in } \Omega, \\ \text{div} \phi = 0 & \text{in } \Omega, \\ \phi \cdot \mathbf{n} = 0 & \text{on } \Gamma, \\ \mathbf{curl} \phi = \mathbf{0} & \text{on } \Gamma. \end{cases} \quad (3.7)$$

After the determination of the velocity  $\mathbf{u} = \mathbf{curl} \phi$ , the pressure  $p$  can be recovered by following the same procedure as in the two-dimensional case, namely by solving subproblem (3.3). For brevity, the details are omitted here.

**Remark 3.2.** For slip boundary condition  $\mathbf{u} = \mathbf{g}$  on  $\Gamma$ , one simply replaces the boundary constraint with  $\phi \cdot \mathbf{n} = 0$  and  $\mathbf{curl} \phi = \mathbf{g}$ .

We now extend our framework to the steady three-dimensional Navier-Stokes problem. As discussed above, applying the curl operator to both sides of (1.2a) effectively decouples the velocity field from the pressure. Since the only difference between the Stokes and Navier-Stokes equations is the presence of the nonlinear advection term, however, Theorem 2.2 gives the result of  $\mathbf{curl}((\mathbf{u} \cdot \nabla)\mathbf{u})$ . Thus, the combination of (3.7) and (2.5) results in the decoupled subproblem for the velocity:

$$\begin{cases} \nu\Delta^2\phi + (\Delta\phi \cdot \nabla)\mathbf{curl} \phi - (\mathbf{curl} \phi \cdot \nabla)\Delta\phi = \mathbf{curl} \mathbf{f} & \text{in } \Omega, \\ \text{div} \phi = 0 & \text{in } \Omega, \\ \phi \cdot \mathbf{n} = 0 & \text{on } \Gamma, \\ \mathbf{curl} \phi = \mathbf{0} & \text{on } \Gamma. \end{cases} \quad (3.8)$$

Similarly, the decoupled pressure subproblem is formulated as (3.5).

**Remark 3.3.** In the earlier works [24, 40], E and Liu developed the finite difference method and finite element method to solve the Navier-Stokes based on the vorticity-vector potential formulations, which typically require the simultaneous approximation of multiple fields (potential and vorticity). Building upon these studies, our approach departs from the classical formulations by further exploiting properties of the curl operator on (2.7). This leads to the decoupled formulation (3.8), which is characterized by a single unknown  $\phi$ . On the other hand, this can be viewed as the extension of “pure” stream function formulation (Eqs. (1.5a)–(1.5b) in [39] or (3.4) in this manuscript) in three dimensions.

It is noted that the decoupled subproblems for the Stokes and Navier–Stokes equations require higher regularity, but the challenges associated with high-order derivatives can be effectively addressed by machine learning methods through automatic differentiation and neural network parameterizations. The specific machine learning algorithm used to solve these decoupled subproblems is presented in the next section. Moreover, we mention that all the above derivations can also be applied to attack unsteady Stokes and Navier–Stokes problems in a straightforward way.

## 4 The Neural networks basis method for incompressible flows

In this section, we first briefly review the TransNet, a special neural networks basis method for solving PDEs, as introduced in [58]. We emphasize that the deduction given below can be extended to any other neural networks basis method.

Mathematically, a single hidden layer fully-connected neural network can be formulated as

$$u_{\text{NN}}(\mathbf{x}) = \alpha_0 + \sum_{m=1}^M \alpha_m \sigma(\mathbf{w}_m^T \mathbf{x} + b_m), \quad (4.1)$$

where  $\sigma(\cdot)$  denotes the nonlinear activation function.  $\mathbf{w}_m \in \mathbb{R}^d$  and  $b_m \in \mathbb{R}$  are the weights and bias of the  $m$ -th hidden neuron, respectively. The vector  $\boldsymbol{\alpha} = [\alpha_0, \alpha_1, \dots, \alpha_M]^T$  are the parameters including the weights and bias of the output layer. Here,  $M$  is the width of  $u_{\text{NN}}(\mathbf{x})$ .

In neural networks basis method, the parameters  $\mathbf{w}_m$  and  $b_m$  are fixed for all  $m$ . Consequently, each hidden neuron acts as a fixed nonlinear basis function over the domain. We define the neural feature space as

$$V_M = \text{span}\{\psi_0, \psi_1, \dots, \psi_M\},$$

where  $\psi_0 = 1$  and  $\psi_m = \sigma(\mathbf{w}_m^T \mathbf{x} + b_m)$  for  $m = 1, \dots, M$ . Since  $u_{\text{NN}}(\mathbf{x}) \in V_M$ , the training process reduces to determining the optimal output coefficients  $\boldsymbol{\alpha}$ .

The initialization of hidden layer weights and biases remains a critical issue for neural network basis methods. TransNet addresses this challenge by adopting a special strategy that ensures hidden layer neurons are uniformly distributed within the unit ball. In the present work, we employ the same initialization strategy, which is summarized in the following steps.

1. Reparameterize each neural feature into the form

$$\sigma(\mathbf{w}_m^T \mathbf{x} + b_m) = \sigma(\gamma_m(\mathbf{s}_m^T \mathbf{x} + r_m)),$$

where  $\gamma_m = \|\mathbf{w}_m\|_2$ ,  $\mathbf{s}_m = \mathbf{w}_m/\gamma_m$ ,  $r_m = b_m/\gamma_m$ . Then, one turn to initialize the parameters  $\mathbf{s}_m$ ,  $r_m$  and  $\gamma_m$ ,  $m = 1, \dots, M$ .

2. Pre-set the parameters  $\mathbf{s}_m$  and  $r_m$  as follows.

$$\mathbf{s}_m = \frac{\mathbf{X}_m}{\|\mathbf{X}_m\|_2}, \quad r_m = U_m, \quad 1 \leq m \leq M,$$

where  $\mathbf{X}_m$  are i.i.d.  $d$ -dimensional standard Gaussian random variables and  $U_m$  are i.i.d. uniform random variables on  $[0, 1]$ . This approach yields a set of uniformly distributed partition hyperplanes within the unit ball  $B(0) = \{\mathbf{x} : \|\mathbf{x}\|_2 \leq 1\} \subset \mathbb{R}^d$ .

3. Assume  $\gamma = \gamma_m$  for  $m = 1, \dots, M$  for simplicity. One will use realizations of Gaussian random fields as auxiliary functions to tune the shape parameter  $\gamma$  without utilizing any information about PDEs. We refer to Algorithm 1 in [58] for details.

While the preceding formulation describes a scalar-valued neural network, it can be naturally extended to vector-valued functions. For a function  $\Phi_{\text{NN}}(\mathbf{x}) : \mathbb{R}^d \rightarrow \mathbb{R}^k$ , each component  $\Phi_i$  is represented by a scalar neural network of the form (4.1). To enhance computational efficiency, all components share the same set of hidden-layer basis functions, that is, identical weights  $\mathbf{w}_m$  and biases  $b_m$ , while maintaining independent output coefficients  $\alpha^{(i)} \in \mathbb{R}^{M+1}$  for each component.

In the remainder of this section, we detail the algorithmic implementation of the proposed framework for solving the steady Stokes and Navier-Stokes equations. In particular, we leverage the TransNet architecture to solve the decoupled, structure-preserving formulations derived in Section 2.

#### 4.1 The steady Stokes problem

Generally speaking, we parameterize the stream function  $\phi$  in two-dimensions or the vector potential  $\boldsymbol{\phi}$  in three-dimensions, using the neural network  $\phi_{\text{NN}}$  or  $\Phi_{\text{NN}}$ , respectively. By imposing the subproblems (3.2) or (3.7) at collocation points, we obtain a least squares problem with respect to the output coefficients  $\boldsymbol{\alpha}$  or  $[\alpha_1, \alpha_2, \alpha_3]^T$ . Once the velocity field is resolved, the corresponding pressure can be efficiently recovered through the decoupled subproblem (3.3) within the TransNet framework. In the following, we denote  $\|\cdot\|_2$  as the vector  $l^2$ -norm in Euclidian space.

We first consider the two-dimensional Stokes problem. Since the single hidden layer fully-connected neural networks have sufficient expressive power for approximating low-dimensional functions [2, 30], we approximate the stream function  $\phi$  in (3.2) by the neural network  $\phi_{\text{NN}}$  as defined by (4.1). To discretize the problem, we choose the collocation points  $\mathbf{X}^{in} = \{\mathbf{x}_i^{in}\}_{i=1}^I \subset \Omega$  and  $\mathbf{X}^{bd} = \{\mathbf{x}_j^{bd}\}_{j=1}^J \subset \Gamma$ . We then proceed to solve the resulting system

$$\begin{cases} \nu \Delta^2 \sum_{m=0}^M \alpha_m \psi_m(\mathbf{x}_i^{in}) = \text{curl } \mathbf{f}(\mathbf{x}_i^{in}) & i = 1, \dots, I, \\ \sum_{m=0}^M \alpha_m \psi_m(\mathbf{x}_j^{bd}) = 0 & j = 1, \dots, J, \\ \frac{\partial}{\partial n} \sum_{m=0}^M \alpha_m \psi_m(\mathbf{x}_j^{bd}) = 0, & j = 1, \dots, J. \end{cases} \quad (4.2)$$

Following the linearity of the differential operator, we can reformulate (4.2) as

$$\begin{bmatrix} \nu \Delta^2 \boldsymbol{\Psi}_{in} \\ \boldsymbol{\Psi}_{bd} \\ \partial_n \boldsymbol{\Psi}_{bd} \end{bmatrix} \boldsymbol{\alpha} = \begin{bmatrix} \text{curl } \mathbf{F} \\ \mathbf{0} \\ \mathbf{0} \end{bmatrix}, \quad (4.3)$$

where

$$\begin{aligned} \Delta^2 \boldsymbol{\Psi}_{in} &= [\Delta^2 \psi_m(\mathbf{x}_i^{in})] \in \mathbb{R}^{I \times (M+1)}, & \text{curl } \mathbf{F} &= [\text{curl } \mathbf{f}(\mathbf{x}_i^{in})] \in \mathbb{R}^I \\ \boldsymbol{\Psi}_{bd} &= [\psi_m(\mathbf{x}_j^{bd})] \in \mathbb{R}^{J \times (M+1)}, & \partial_n \boldsymbol{\Psi}_{bd} &= [\partial_n \psi_m(\mathbf{x}_j^{bd})] \in \mathbb{R}^{J \times (M+1)}. \end{aligned}$$

Typically, (4.3) is an over-determined system. Therefore, we solve the corresponding least-squares problem

$$\min_{\boldsymbol{\alpha}} \left\| \begin{bmatrix} \nu \Delta^2 \boldsymbol{\Psi}_{in} \\ \boldsymbol{\Psi}_{bd} \\ \partial_n \boldsymbol{\Psi}_{bd} \end{bmatrix} \boldsymbol{\alpha} - \begin{bmatrix} \text{curl } \mathbf{F} \\ \mathbf{0} \\ \mathbf{0} \end{bmatrix} \right\|_2^2, \quad (4.4)$$

which can be solved using the linear solvers provided by NumPy. If we denote  $\boldsymbol{\alpha}^*$  as the minimizer of (4.4), then the approximate velocity  $\mathbf{u}_{\text{NN}}$  is given by

$$\mathbf{u}_{\text{NN}} = [u_1^*, u_2^*]^T = \begin{bmatrix} \sum_{m=0}^M \alpha_m^* \partial_y \psi_m \\ -\sum_{m=0}^M \alpha_m^* \partial_x \psi_m \end{bmatrix}.$$





appendix. Subsequently, the neural network basis method is employed to solve these linearized equations. This strategy is referred to as the Newton-LLSQ framework, as proposed in [16]. By approximating the stream function in two dimensions or the vector potential in three dimensions and enforcing the interior and boundary conditions at collocation points, each iteration reduces to solving a linear least-squares system for the coefficients  $\boldsymbol{\alpha}$ . This approach is equivalent to first deriving a discretized nonlinear system and then applying the Gauss-Newton method to solve it [32].

To address the nonlinearity of the Navier-Stokes equations, we follow the idea in [32] and linearize the convection term via variational derivatives. For the nonlinear advection operator  $f(\mathbf{u}) = (\mathbf{u} \cdot \nabla)\mathbf{u}$ , the Gâteaux derivative (see [8]) of  $f$  at  $\mathbf{u}$  in any direction  $\mathbf{v}$  is defined as

$$\mathcal{D}f(\mathbf{u})[\mathbf{v}] = \lim_{\varepsilon \rightarrow 0} \frac{f(\mathbf{u} + \varepsilon\mathbf{v}) - f(\mathbf{u})}{\varepsilon}.$$

A straightforward expansion yields

$$\mathcal{D}f(\mathbf{u})[\mathbf{v}] = \lim_{\varepsilon \rightarrow 0} \frac{(\mathbf{u} \cdot \nabla)\varepsilon\mathbf{v} + (\varepsilon\mathbf{v} \cdot \nabla)\mathbf{u} + (\varepsilon\mathbf{v} \cdot \nabla)\varepsilon\mathbf{v}}{\varepsilon} = (\mathbf{u} \cdot \nabla)\mathbf{v} + (\mathbf{v} \cdot \nabla)\mathbf{u}.$$

It is worth emphasizing that the mapping  $\mathbf{v} \mapsto \mathcal{D}f(\mathbf{u})[\mathbf{v}]$  is linear and continuous with respect to  $\mathbf{v}$  in Sobolev spaces. Therefore, the Gâteaux derivative coincides with the Fréchet derivative of  $f$  at  $\mathbf{u}$  [8]. Based on this result, the standard Newton linearization of the convection term at the  $(k+1)$ -th iteration reads

$$\begin{aligned} f(\mathbf{u}^{(k+1)}) &\approx f(\mathbf{u}^{(k)}) + \mathcal{D}f(\mathbf{u}^{(k)})[\delta\mathbf{u}] \\ &= (\mathbf{u}^{(k)} \cdot \nabla)\mathbf{u}^{(k)} + (\mathbf{u}^{(k)} \cdot \nabla)\delta\mathbf{u} + (\delta\mathbf{u} \cdot \nabla)\mathbf{u}^{(k)} \\ &= \mathbf{u}^{(k)} \cdot \nabla\mathbf{u}^{(k+1)} + \mathbf{u}^{(k+1)} \cdot \nabla\mathbf{u}^{(k)} - \mathbf{u}^{(k)} \cdot \nabla\mathbf{u}^{(k)}, \end{aligned} \quad (4.10)$$

where  $\delta\mathbf{u} = \mathbf{u}^{(k+1)} - \mathbf{u}^{(k)}$ .

Specifically, in the two-dimensional case, we employ the stream function representation  $\mathbf{u} = \mathbf{curl} \phi$ . Substituting the linearized term (4.10) into the decoupled velocity subproblem (3.4), we obtain the linearized problem at each iteration step as follows:

$$\mu\Delta^2\phi^{(k+1)} - (\mathbf{curl} \phi^{(k)} \cdot \nabla)\Delta\phi^{(k+1)} - (\mathbf{curl} \phi^{(k+1)} \cdot \nabla)\Delta\phi^{(k)} = \mathbf{curl} \mathbf{f} - (\mathbf{curl} \phi^{(k)} \cdot \nabla)\Delta\phi^{(k)}. \quad (4.11)$$

Similarly, in the three-dimensional case, where  $\mathbf{u} = \mathbf{curl} \phi$ , substituting the linearized term (4.10) into the corresponding subproblem (3.8) yields

$$\begin{aligned} &\mu\Delta^2\phi^{(k+1)} - (\mathbf{curl} \phi^{(k)} \cdot \nabla)\Delta\phi^{(k+1)} + (\Delta\phi^{(k)} \cdot \nabla)\mathbf{curl} \phi^{(k+1)} \\ &\quad - (\mathbf{curl} \phi^{(k+1)} \cdot \nabla)\Delta\phi^{(k)} + (\Delta\phi^{(k+1)} \cdot \nabla)\mathbf{curl} \phi^{(k)} \\ &= \mathbf{curl} \mathbf{f} - (\mathbf{curl} \phi^{(k)} \cdot \nabla)\Delta\phi^{(k)} + (\Delta\phi^{(k)} \cdot \nabla)\mathbf{curl} \phi^{(k)}. \end{aligned} \quad (4.12)$$

Next, we implement the Decoupled-DFNN framework for the Navier-Stokes equations. In the two-dimensional case, we first approximate the stream function  $\phi$  using the neural network  $\phi_{\text{NN}}$ . Substituting the (4.11) into the (3.4) and selecting collocation points  $\mathbf{X}^{in} = \{\mathbf{x}_i^{in}\}_{i=1}^I \subset \Omega$  and  $\mathbf{X}^{bd} = \{\mathbf{x}_j^{bd}\}_{j=1}^J \subset \Gamma$ , the problem is reduced to determining the optimal coefficients  $\boldsymbol{\alpha}^{(k+1)}$  that satisfy the following system

$$\left\{ \begin{array}{l} \nu\Delta^2 \sum_{m=0}^M \alpha_m^{(k+1)} \psi_m(\mathbf{x}_i^{in}) - (\mathbf{curl} \sum_{m=0}^M \alpha_m^{(k)} \psi_m(\mathbf{x}_i^{in}) \cdot \nabla)\Delta \sum_{m=0}^M \alpha_m^{(k+1)} \psi_m(\mathbf{x}_i^{in}) \\ \quad - (\mathbf{curl} \sum_{m=0}^M \alpha_m^{(k+1)} \psi_m(\mathbf{x}_i^{in}) \cdot \nabla)\Delta \sum_{m=0}^M \alpha_m^{(k)} \psi_m(\mathbf{x}_i^{in}) \\ = \mathbf{curl} \mathbf{f} - (\mathbf{curl} \sum_{m=0}^M \alpha_m^{(k)} \psi_m(\mathbf{x}_i^{in}) \cdot \nabla)\Delta \sum_{m=0}^M \alpha_m^{(k)} \psi_m(\mathbf{x}_i^{in}), \quad i = 1 \cdots, I, \\ \sum_{m=0}^M \alpha_m^{(k+1)} \psi_m(\mathbf{x}_j^{bd}) = 0, \quad j = 1 \cdots, J, \\ \frac{\partial}{\partial n} \sum_{m=0}^M \alpha_m^{(k+1)} \psi_m(\mathbf{x}_j^{bd}) = 0, \quad j = 1 \cdots, J. \end{array} \right.$$

To represent this system in matrix form, denote  $\odot$  the standard Hadamard product for matrices of the same dimensions, and extend this operator to the case of a vector  $\mathbf{a} \in \mathbb{R}^m$  and a matrix  $\mathbf{B} \in \mathbb{R}^{m \times n}$ . Specifically, for  $\mathbf{C} = \mathbf{a} \odot \mathbf{B}$ , the entries are defined by  $c_{ij} = a_i b_{ij}$ . This operation can be expressed in terms of standard matrix multiplication as

$$\mathbf{C} = \text{diag}(\mathbf{a})\mathbf{B},$$

where  $\text{diag}(\mathbf{a})$  is the  $m \times m$  diagonal matrix with the elements of  $\mathbf{a}$  on its main diagonal. Using this notation, we reformulate the system into the following block matrix form

$$\begin{bmatrix} \nu \Delta^2 \Psi_{in} + \mathbf{NL} \\ \Psi_{bd} \\ \partial_n \Psi_{bd} \end{bmatrix} \boldsymbol{\alpha}^{(k+1)} = \begin{bmatrix} \tilde{\mathbf{F}} \\ \mathbf{0} \\ \mathbf{0} \end{bmatrix}, \quad (4.13)$$

where

$$\begin{aligned} \mathbf{NL} &= -\mathbf{U}_1^{(k)} \odot \partial_x \Delta \Psi_{in} - \mathbf{U}_2^{(k)} \odot \partial_y \Delta \Psi_{in} + \Delta \mathbf{U}_2^{(k)} \odot \partial_y \Psi_{in} + \Delta \mathbf{U}_1^{(k)} \odot \partial_x \Psi_{in}, \\ \tilde{\mathbf{F}} &= \text{curl } \mathbf{F} + \mathbf{U}_1^{(k)} \odot \Delta \mathbf{U}_2^{(k)} - \mathbf{U}_2^{(k)} \odot \Delta \mathbf{U}_1^{(k)}, \quad \text{curl } \mathbf{F} = [\text{curl } \mathbf{f}(\mathbf{x}_i^{in})] \in \mathbb{R}^I, \\ \mathbf{U}_1^k &= \partial_y \Psi_{in} \cdot \boldsymbol{\alpha}^{(k)}, \quad \Delta \mathbf{U}_1^k = \partial_y \Delta \Psi_{in} \cdot \boldsymbol{\alpha}^{(k)}, \\ \mathbf{U}_2^k &= -\partial_x \Psi_{in} \cdot \boldsymbol{\alpha}^{(k)}, \quad \Delta \mathbf{U}_2^k = -\partial_x \Delta \Psi_{in} \cdot \boldsymbol{\alpha}^{(k)}, \\ \Delta^2 \Psi_{in} &= [\Delta^2 \psi_m(\mathbf{x}_i^{in})] \in \mathbb{R}^{I \times (M+1)}, \\ \partial_x \Delta \Psi_{in} &= [\partial_x \Delta \psi_m(\mathbf{x}_i^{in})] \in \mathbb{R}^{I \times (M+1)}, \quad \partial_y \Delta \Psi_{in} = [\partial_y \Delta \psi_m(\mathbf{x}_i^{in})] \in \mathbb{R}^{I \times (M+1)}, \\ \partial_x \Psi_{in} &= [\partial_x \psi_m(\mathbf{x}_i^{in})] \in \mathbb{R}^{I \times (M+1)}, \quad \partial_y \Psi_{in} = [\partial_y \psi_m(\mathbf{x}_i^{in})] \in \mathbb{R}^{I \times (M+1)}, \\ \Psi_{bd} &= [\psi_m(\mathbf{x}_j^{bd})] \in \mathbb{R}^{J \times (M+1)}, \quad \partial_n \Psi_{bd} = [\partial_n \psi_m(\mathbf{x}_j^{bd})] \in \mathbb{R}^{J \times (M+1)}. \end{aligned}$$

Since (4.13) is an over-determined system, we solve the corresponding least-squares problem

$$\min_{\boldsymbol{\alpha}^{(k+1)}} \left\| \begin{bmatrix} \nu \Delta^2 \Psi_{in} + \mathbf{NL} \\ \Psi_{bd} \\ \partial_n \Psi_{bd} \end{bmatrix} \boldsymbol{\alpha}^{(k+1)} - \begin{bmatrix} \tilde{\mathbf{F}} \\ \mathbf{0} \\ \mathbf{0} \end{bmatrix} \right\|_2^2. \quad (4.14)$$

Once the minimizer  $\boldsymbol{\alpha}^*$  is obtained, the solution to (3.5) can be approximated as

$$\begin{bmatrix} \partial_x \Psi_{in} \\ \partial_y \Psi_{in} \\ \Psi_0^T \end{bmatrix} \boldsymbol{\beta} = \begin{bmatrix} \tilde{\mathbf{F}}_1 \\ \tilde{\mathbf{F}}_2 \\ 0 \end{bmatrix}, \quad (4.15)$$

where

$$\begin{aligned} \tilde{\mathbf{F}}_1 &= [f_1(\mathbf{x}_i^{in}) + \nu \Delta u_1^*(\mathbf{x}_i^{in}) - (u_1 \partial_x u_1 + u_2 \partial_y u_1)] \in \mathbb{R}^I, \\ \tilde{\mathbf{F}}_2 &= [f_2(\mathbf{x}_i^{in}) + \nu \Delta u_2^*(\mathbf{x}_i^{in}) - (u_1 \partial_x u_2 + u_2 \partial_y u_2)] \in \mathbb{R}^I, \\ \Psi_0 &= [\psi_m(\mathbf{x}_0)] \in \mathbb{R}^{M+1}. \end{aligned}$$

Similarly, the system (4.15) is reformulated as a least-squares problem, from which we compute the minimize  $\boldsymbol{\beta}^*$ . The pressure is then approximated by  $p_{\text{NN}} = \sum_{m=0}^M \beta_m^* \psi_m(\mathbf{x})$ .

For the three-dimensional case, we approximate the potential function  $\phi$  using the neural network

$$\phi_{\text{NN}} = [\phi_{1,\text{NN}}, \phi_{2,\text{NN}}, \phi_{3,\text{NN}}]^T = \left[ \sum_{m=0}^M \alpha_{1,m} \phi_m, \sum_{m=0}^M \alpha_{2,m} \phi_m, \sum_{m=0}^M \alpha_{3,m} \phi_m \right]^T.$$

Substituting the (4.12) into the (3.8) and discretizing the resulting equations at the collocation points  $\mathbf{X}^{in} = \{\mathbf{x}_i^{in}\}_{i=1}^I \subset \Omega$  and  $\mathbf{X}^{bd} = \{\mathbf{x}_j^{bd}\}_{j=1}^J \subset \Gamma$ , we obtain

$$\left\{ \begin{array}{l} \mu \Delta^2 \phi_{\text{NN}}^{(k+1)}(\mathbf{x}_i^{in}) - (\mathbf{curl} \phi_{\text{NN}}^{(k)}(\mathbf{x}_i^{in}) \cdot \nabla) \Delta \phi_{\text{NN}}^{(k+1)}(\mathbf{x}_i^{in}) + (\Delta \phi_{\text{NN}}^{(k)}(\mathbf{x}_i^{in}) \cdot \nabla) \mathbf{curl} \phi_{\text{NN}}^{(k+1)}(\mathbf{x}_i^{in}) \\ \quad - (\mathbf{curl} \phi_{\text{NN}}^{(k+1)}(\mathbf{x}_i^{in}) \cdot \nabla) \Delta \phi_{\text{NN}}^{(k)}(\mathbf{x}_i^{in}) + (\Delta \phi_{\text{NN}}^{(k+1)}(\mathbf{x}_i^{in}) \cdot \nabla) \mathbf{curl} \phi_{\text{NN}}^{(k)}(\mathbf{x}_i^{in}) \\ = \mathbf{curl} \mathbf{f} - (\mathbf{curl} \phi_{\text{NN}}^{(k)}(\mathbf{x}_i^{in}) \cdot \nabla) \Delta \phi_{\text{NN}}^{(k)}(\mathbf{x}_i^{in}) + (\Delta \phi_{\text{NN}}^{(k)}(\mathbf{x}_i^{in}) \cdot \nabla) \mathbf{curl} \phi_{\text{NN}}^{(k)}(\mathbf{x}_i^{in}), \quad i = 1, \dots, I, \\ \text{div} \phi_{\text{NN}}^{(k+1)}(\mathbf{x}_i^{in}) = 0 \quad i = 1, \dots, I, \\ \phi_{\text{NN}}^{(k+1)}(\mathbf{x}_j^{bd}) \cdot \mathbf{n}(\mathbf{x}_j^{bd}) = 0 \quad j = 1, \dots, J, \\ \mathbf{curl} \phi_{\text{NN}}^{(k+1)}(\mathbf{x}_j^{bd}) = \mathbf{0} \quad j = 1, \dots, J, \end{array} \right.$$

which can be further reformulated in block matrix form

$$\begin{bmatrix} \nu \Delta^2 \Psi_{in} + N_{11} & N_{12} & N_{13} \\ N_{21} & \nu \Delta^2 \Psi_{in} + N_{22} & N_{23} \\ N_{31} & N_{32} & \nu \Delta^2 \Psi_{in} + N_{33} \\ \partial_x \Psi_{in} & \partial_y \Psi_{in} & \partial_z \Psi_{in} \\ \Psi_{bd} \mathbf{n}_1 & \Psi_{bd} \mathbf{n}_2 & \Phi_{bd} \mathbf{n}_3 \\ \partial_z \Psi_{bd} & -\partial_z \Psi_{bd} & \partial_y \Psi_{bd} \\ -\partial_y \Psi_{bd} & \partial_x \Psi_{bd} & -\partial_x \Psi_{bd} \end{bmatrix} \begin{bmatrix} \alpha_1^{(k+1)} \\ \alpha_2^{(k+1)} \\ \alpha_3^{(k+1)} \end{bmatrix} = \begin{bmatrix} \tilde{F}_1 \\ \tilde{F}_2 \\ \tilde{F}_3 \\ \mathbf{0} \\ \mathbf{0} \\ \mathbf{0} \\ \mathbf{0} \end{bmatrix}, \quad (4.16)$$

where

$$\begin{aligned} N_{11} &= -(\mathbf{U}_1^{(k)} \odot \partial_x \Delta \Psi_{in} + \mathbf{U}_2^{(k)} \odot \partial_y \Delta \Psi_{in} + \mathbf{U}_3^{(k)} \odot \partial_z \Delta \Psi_{in}) \\ &\quad - (\partial_y \Delta \Psi_{in} \cdot \alpha_1^{(k)} \odot \partial_z \Psi_{in} - \partial_z \Delta \Psi_{in} \cdot \alpha_1^{(k)} \odot \partial_y \Psi_{in}) + \partial_x \mathbf{U}_1^{(k)} \odot \Delta \Psi_{in}, \\ N_{12} &= -\Delta \Psi_{in} \cdot \alpha_1^{(k)} \odot \partial_{xz} \Psi_{in} - \Delta \Psi_{in} \cdot \alpha_2^{(k)} \odot \partial_{yz} \Psi_{in} - \Delta \Psi_{in} \cdot \alpha_3^{(k)} \odot \partial_{zz} \Psi_{in} \\ &\quad - (\partial_z \Delta \Psi_{in} \cdot \alpha_1^{(k)} \odot \partial_x \Psi_{in} - \partial_x \Delta \Psi_{in} \cdot \alpha_1^{(k)} \odot \partial_z \Psi_{in}) + \partial_y \mathbf{U}_1^{(k)} \odot \Delta \Psi_{in}, \\ N_{13} &= \Delta \Psi_{in} \cdot \alpha_1^{(k)} \odot \partial_{xy} \Psi_{in} + \Delta \Psi_{in} \cdot \alpha_2^{(k)} \odot \partial_{yy} \Psi_{in} + \Delta \Psi_{in} \cdot \alpha_3^{(k)} \odot \partial_{zy} \Psi_{in} \\ &\quad - (\partial_x \Delta \Psi_{in} \cdot \alpha_1^{(k)} \odot \partial_y \Psi_{in} - \partial_y \Delta \Psi_{in} \cdot \alpha_1^{(k)} \odot \partial_x \Psi_{in}) + \partial_z \mathbf{U}_1^{(k)} \odot \Delta \Psi_{in}, \\ N_{21} &= \Delta \Psi_{in} \cdot \alpha_1^{(k)} \odot \partial_{xz} \Psi_{in} + \Delta \Psi_{in} \cdot \alpha_2^{(k)} \odot \partial_{yz} \Psi_{in} + \Delta \Psi_{in} \cdot \alpha_3^{(k)} \odot \partial_{zz} \Psi_{in} \\ &\quad - (\partial_y \Delta \Psi_{in} \cdot \alpha_2^{(k)} \odot \partial_z \Psi_{in} - \partial_z \Delta \Psi_{in} \cdot \alpha_2^{(k)} \odot \partial_y \Psi_{in}) + \partial_x \mathbf{U}_2^{(k)} \odot \Delta \Psi_{in}, \\ N_{22} &= -(\mathbf{U}_1^{(k)} \odot \partial_x \Delta \Psi_{in} + \mathbf{U}_2^{(k)} \odot \partial_y \Delta \Psi_{in} + \mathbf{U}_3^{(k)} \odot \partial_z \Delta \Psi_{in}) \\ &\quad - (\partial_z \Delta \Psi_{in} \cdot \alpha_2^{(k)} \odot \partial_x \Psi_{in} - \partial_x \Delta \Psi_{in} \cdot \alpha_2^{(k)} \odot \partial_z \Psi_{in}) + \partial_y \mathbf{U}_2^{(k)} \odot \Delta \Psi_{in} \\ N_{23} &= -\Delta \Psi_{in} \cdot \alpha_1^{(k)} \odot \partial_{xx} \Psi_{in} - \Delta \Psi_{in} \cdot \alpha_2^{(k)} \odot \partial_{yx} \Psi_{in} - \Delta \Psi_{in} \cdot \alpha_3^{(k)} \odot \partial_{zx} \Psi_{in} \\ &\quad - (\partial_x \Delta \Psi_{in} \cdot \alpha_2^{(k)} \odot \partial_y \Psi_{in} - \partial_y \Delta \Psi_{in} \cdot \alpha_2^{(k)} \odot \partial_x \Psi_{in}) + \partial_z \mathbf{U}_2^{(k)} \odot \Delta \Psi_{in}, \\ N_{31} &= -(\Delta \Psi_{in} \cdot \alpha_1^{(k)} \odot \partial_{xy} \Psi_{in} + \Delta \Psi_{in} \cdot \alpha_2^{(k)} \odot \partial_{yy} \Psi_{in} + \Delta \Psi_{in} \cdot \alpha_3^{(k)} \odot \partial_{zy} \Psi_{in}) \\ &\quad - (\partial_y \Delta \Psi_{in} \cdot \alpha_3^{(k)} \odot \partial_z \Psi_{in} - \partial_z \Delta \Psi_{in} \cdot \alpha_3^{(k)} \odot \partial_y \Psi_{in}) + \partial_x \mathbf{U}_3^{(k)} \odot \Delta \Psi_{in}, \\ N_{32} &= \Delta \Psi_{in} \cdot \alpha_1^{(k)} \odot \partial_{xx} \Psi_{in} + \Delta \Psi_{in} \cdot \alpha_2^{(k)} \odot \partial_{yx} \Psi_{in} + \Delta \Psi_{in} \cdot \alpha_3^{(k)} \odot \partial_{zx} \Psi_{in} \\ &\quad - (\partial_z \Delta \Psi_{in} \cdot \alpha_3^{(k)} \odot \partial_x \Psi_{in} - \partial_x \Delta \Psi_{in} \cdot \alpha_3^{(k)} \odot \partial_z \Psi_{in}) + \partial_y \mathbf{U}_3^{(k)} \odot \Delta \Psi_{in}, \\ N_{33} &= -(\mathbf{U}_1^{(k)} \odot \partial_x \Delta \Psi_{in} + \mathbf{U}_2^{(k)} \odot \partial_y \Delta \Psi_{in} + \mathbf{U}_3^{(k)} \odot \partial_z \Delta \Psi_{in}) \\ &\quad - (\partial_x \Delta \Psi_{in} \cdot \alpha_3^{(k)} \odot \partial_y \Psi_{in} - \partial_y \Delta \Psi_{in} \cdot \alpha_3^{(k)} \odot \partial_x \Psi_{in}) + \partial_z \mathbf{U}_3^{(k)} \odot \Delta \Psi_{in}, \end{aligned}$$

$$\begin{aligned}
\tilde{F}_1 &= \partial_y F_3 - \partial_z F_2 - (U_1^{(k)} \odot \partial_x \Delta \Psi_{in} \cdot \alpha_1^{(k)} + U_2^{(k)} \odot \partial_y \Delta \Psi_{in} \cdot \alpha_1^{(k)} + U_3^{(k)} \odot \partial_x \Delta \Psi_{in} \cdot \alpha_1^{(k)}) \\
&\quad + (\partial_x U_1^{(k)} \odot \Delta \Psi_{in} \cdot \alpha_1^{(k)} + \partial_y U_1^{(k)} \odot \Delta \Psi_{in} \cdot \alpha_2^{(k)} + \partial_z U_1^{(k)} \odot \Delta \Psi_{in} \cdot \alpha_3^{(k)}), \\
\tilde{F}_2 &= \partial_z F_1 - \partial_x F_3 - (U_1^{(k)} \odot \partial_x \Delta \Psi_{in} \cdot \alpha_2^{(k)} + U_2^{(k)} \odot \partial_y \Delta \Psi_{in} \cdot \alpha_2^{(k)} + U_3^{(k)} \odot \partial_x \Delta \Psi_{in} \cdot \alpha_2^{(k)}) \\
&\quad + (\partial_x U_2^{(k)} \odot \Delta \Psi_{in} \cdot \alpha_1^{(k)} + \partial_y U_2^{(k)} \odot \Delta \Psi_{in} \cdot \alpha_2^{(k)} + \partial_z U_2^{(k)} \odot \Delta \Psi_{in} \cdot \alpha_3^{(k)}), \\
\tilde{F}_3 &= \partial_x F_2 - \partial_y F_1 - (U_1^{(k)} \odot \partial_x \Delta \Psi_{in} \cdot \alpha_3^{(k)} + U_2^{(k)} \odot \partial_y \Delta \Psi_{in} \cdot \alpha_3^{(k)} + U_3^{(k)} \odot \partial_x \Delta \Psi_{in} \cdot \alpha_3^{(k)}) \\
&\quad + (\partial_x U_3^{(k)} \odot \Delta \Psi_{in} \cdot \alpha_1^{(k)} + \partial_y U_3^{(k)} \odot \Delta \Psi_{in} \cdot \alpha_2^{(k)} + \partial_z U_3^{(k)} \odot \Delta \Psi_{in} \cdot \alpha_3^{(k)}).
\end{aligned}$$

Here,

$$\begin{aligned}
U_1^{(k)} &= \partial_y \Psi_{in} \cdot \alpha_3^{(k)} - \partial_z \Psi_{in} \cdot \alpha_2^{(k)}, & \partial_r U_1^{(k)} &= \partial_{ry} \Psi_{in} \cdot \alpha_3^{(k)} - \partial_{rz} \Psi_{in} \cdot \alpha_2^{(k)}, \quad r = x, y, z, \\
U_2^{(k)} &= \partial_z \Psi_{in} \cdot \alpha_1^{(k)} - \partial_x \Psi_{in} \cdot \alpha_3^{(k)}, & \partial_r U_2^{(k)} &= \partial_{rz} \Psi_{in} \cdot \alpha_1^{(k)} - \partial_{rx} \Psi_{in} \cdot \alpha_3^{(k)}, \quad r = x, y, z, \\
U_3^{(k)} &= \partial_x \Psi_{in} \cdot \alpha_2^{(k)} - \partial_y \Psi_{in} \cdot \alpha_1^{(k)}, & \partial_r U_3^{(k)} &= \partial_{rx} \Psi_{in} \cdot \alpha_2^{(k)} - \partial_{ry} \Psi_{in} \cdot \alpha_1^{(k)}, \quad r = x, y, z,
\end{aligned}$$

$$\begin{aligned}
\Delta \Psi_{in} &= [\Delta \psi_m(\mathbf{x}_i^{in})] \in \mathbb{R}^{I \times (M+1)}, & \partial_r \Psi_{in} &= [\partial_s \psi_m(\mathbf{x}_i^{in})] \in \mathbb{R}^{I \times (M+1)}, \quad r = x, y, z, \\
\Delta^2 \Psi_{in} &= [\Delta^2 \psi_m(\mathbf{x}_i^{in})] \in \mathbb{R}^{I \times (M+1)}, & \partial_{\iota r} \Psi_{in} &= [\partial_{\iota} \partial_r \psi_m(\mathbf{x}_i^{in})] \in \mathbb{R}^{I \times (M+1)}, \quad \iota, r = x, y, z, \\
\partial_r \Delta \Psi_{in} &= [\partial_r \Delta \psi_m(\mathbf{x}_i^{in})] \in \mathbb{R}^{I \times (M+1)}, \quad r = x, y, z, \\
\Psi_{bd} \mathbf{n}_1 &= [\psi_m(\mathbf{x}_j^{bd}) n_1(\mathbf{x}_j^{bd})] \in \mathbb{R}^{J \times (M+1)}, & \Psi_{bd} \mathbf{n}_2 &= [\psi_m(\mathbf{x}_j^{bd}) n_2(\mathbf{x}_j^{bd})] \in \mathbb{R}^{J \times (M+1)}, \\
\Psi_{bd} \mathbf{n}_3 &= [\psi_m(\mathbf{x}_j^{bd}) n_3(\mathbf{x}_j^{bd})] \in \mathbb{R}^{J \times (M+1)}, & \partial_s \Psi_{bd} &= [\partial_s \psi_m(\mathbf{x}_j^{bd})] \in \mathbb{R}^{J \times (M+1)}, \quad s = x, y, z, \\
\partial_y F_3 - \partial_z F_2 &= [\partial_y f_3(\mathbf{x}_i^{in}) - \partial_z f_2(\mathbf{x}_i^{in})] \in \mathbb{R}^{I \times (M+1)}, \\
\partial_z F_1 - \partial_x F_3 &= [\partial_z f_1(\mathbf{x}_i^{in}) - \partial_x f_3(\mathbf{x}_i^{in})] \in \mathbb{R}^{I \times (M+1)}, \\
\partial_x F_2 - \partial_y F_1 &= [\partial_x f_2(\mathbf{x}_i^{in}) - \partial_y f_1(\mathbf{x}_i^{in})] \in \mathbb{R}^{I \times (M+1)}.
\end{aligned}$$

To solve (4.16), we turn to solve least-squares problem

$$\min_{\alpha^{(k+1)}} \left\| \begin{bmatrix} \nu \Delta^2 \Psi_{in} + N_{11} & N_{12} & N_{13} \\ N_{21} & \nu \Delta^2 \Psi_{in} + N_{22} & N_{23} \\ N_{31} & N_{32} & \nu \Delta^2 \Psi_{in} + N_{33} \\ \partial_x \Psi_{in} & \partial_y \Psi_{in} & \partial_z \Psi_{in} \\ \Psi_{bd} \mathbf{n}_1 & \Psi_{bd} \mathbf{n}_2 & \Phi_{bd} \mathbf{n}_3 \\ & -\partial_z \Psi_{bd} & \partial_y \Psi_{bd} \\ \partial_z \Psi_{bd} & & -\partial_x \Psi_{bd} \\ -\partial_y \Psi_{bd} & \partial_x \Psi_{bd} & \end{bmatrix} \begin{bmatrix} \alpha_1^{(k+1)} \\ \alpha_2^{(k+1)} \\ \alpha_3^{(k+1)} \end{bmatrix} - \begin{bmatrix} \tilde{F}_1 \\ \tilde{F}_2 \\ \tilde{F}_3 \\ \mathbf{0} \\ \mathbf{0} \\ \mathbf{0} \\ \mathbf{0} \\ \mathbf{0} \end{bmatrix} \right\|_2^2. \quad (4.17)$$

Once obtaining the minimizer  $\alpha^*$ , we can reformulate (3.5) to the least-squares problem

$$\min_{\beta} \left\| \begin{bmatrix} \partial_x \Psi_{in} \\ \partial_y \Psi_{in} \\ \partial_z \Psi_{in} \\ \Psi_0^T \end{bmatrix} \beta - \begin{bmatrix} \tilde{F}_1 \\ \tilde{F}_2 \\ \tilde{F}_3 \\ 0 \end{bmatrix} \right\|_2^2, \quad (4.18)$$

where

$$\begin{aligned}
\tilde{F}_1 &= [f_1(\mathbf{x}_i^{in}) + \nu \Delta u_1^*(\mathbf{x}_i^{in}) - (u_1^*(\mathbf{x}_i^{in}) \partial_x u_1^*(\mathbf{x}_i^{in}) + u_2^*(\mathbf{x}_i^{in}) \partial_y u_1^*(\mathbf{x}_i^{in}) + u_3^*(\mathbf{x}_i^{in}) \partial_z u_1^*(\mathbf{x}_i^{in}))] \in \mathbb{R}^I, \\
\tilde{F}_2 &= [f_2(\mathbf{x}_i^{in}) + \nu \Delta u_2^*(\mathbf{x}_i^{in}) - (u_1^*(\mathbf{x}_i^{in}) \partial_x u_2^*(\mathbf{x}_i^{in}) + u_2^*(\mathbf{x}_i^{in}) \partial_y u_2^*(\mathbf{x}_i^{in}) + u_3^*(\mathbf{x}_i^{in}) \partial_z u_2^*(\mathbf{x}_i^{in}))] \in \mathbb{R}^I, \\
\tilde{F}_3 &= [f_3(\mathbf{x}_i^{in}) + \nu \Delta u_3^*(\mathbf{x}_i^{in}) - (u_1^*(\mathbf{x}_i^{in}) \partial_x u_3^*(\mathbf{x}_i^{in}) + u_2^*(\mathbf{x}_i^{in}) \partial_y u_3^*(\mathbf{x}_i^{in}) + u_3^*(\mathbf{x}_i^{in}) \partial_z u_3^*(\mathbf{x}_i^{in}))] \in \mathbb{R}^I, \\
\Psi_0 &= [\psi_m(\mathbf{x}_0)] \in \mathbb{R}^{M+1}.
\end{aligned}$$

The resulting pressure approximation is  $p_{\text{NN}} = \sum_{m=0}^M \beta_m^* \psi_m(\mathbf{x})$ .

### 4.3 Computational complexity

Based on the previous discussion, the final step of the proposed method involves solving an over-determined linear least-squares problem of the form

$$\min_{\mathbf{x}} \|\mathbf{A}\mathbf{x} - \mathbf{b}\|_2^2, \quad (4.19)$$

where  $\mathbf{A} \in \mathbb{R}^{m \times n}$  ( $m \gg n$ ),  $\mathbf{x} \in \mathbb{R}^n$  and  $\mathbf{b} \in \mathbb{R}^n$ . The standard computational complexity for resolving such a system is  $\mathcal{O}(mn^2)$ . Both the current decoupled Decoupled-DFNN and the standard TransNet rely on solving (4.19), their relative efficiency can be compared by analyzing the dimensions of their respective matrices.

In our proposed framework, the velocity and pressure subproblems are solved sequentially, resulting in smaller and independent linear systems. In contrast, the standard TransNet approach solves all variables simultaneously, which leads to a larger coupled system. The computational complexities for the two-dimensional and three-dimensional cases are summarized in Table 4.1, where  $I$  and  $J$  denote the number of interior and boundary collocation points, and  $M$  represents the number of hidden nodes.

Method	Decoupled-DFNN	TransNet
2d	$\mathcal{O}((I + 2J)(M + 1)^2) + \mathcal{O}((2I + 1)(M + 1)^2)$	$\mathcal{O}((3I + 2J)(3M + 3)^2)$
3d	$\mathcal{O}((4I + 4J)(3M + 3)^2) + \mathcal{O}((3I + 1)(M + 1)^2)$	$\mathcal{O}((4I + 3J)(4M + 4)^2)$

Table 4.1: Comparison of computational complexity per iteration for 2D and 3D problems.

## 5 Numerical experiments

In this section, we evaluate the performance of the proposed Decoupled-DFNN method for incompressible flow problems. Our experiments include numerical comparisons of Decoupled-DFNN with both TransNet and PINN. In PINN framework, we shall use the ResNet [29] with width  $M = 30$  and depth  $L = 4$  with an activation function  $\sigma(x) = \tanh(x)$  to approximate the velocity and pressure, and the parameters are determined by the Adam optimizer [38]. To quantify the accuracy of the numerical results, we define the relative  $L^2$  error between the exact solution  $g$  and the neural network approximation  $g_{\text{NN}}$  as

$$\text{error}_g = \frac{\sqrt{\frac{1}{N} \sum_{i=1}^N [g(\mathbf{x}_i) - g_{\text{NN}}(\mathbf{x}_i)]^2}}{\sqrt{\frac{1}{N} \sum_{i=1}^N [g(\mathbf{x}_i)]^2}}.$$

To assess the enforcement of the incompressibility constraint, we further define the absolute divergence error as

$$\text{error}_{\text{div}} = \sqrt{\frac{1}{N} \sum_{i=1}^N [\text{div } \mathbf{g}_{\text{NN}}(\mathbf{x}_i)]^2}.$$

For simplicity, the velocity field is denoted by  $\mathbf{u}(\mathbf{x}) = [u(\mathbf{x}), v(\mathbf{x})]^\top$  for 2D cases, and  $\mathbf{u}(\mathbf{x}) = [u(\mathbf{x}), v(\mathbf{x}), w(\mathbf{x})]^\top$  for 3D case.

All experiments are implemented on a personal laptop equipped with an Intel Core i9-12900H (2.50 GHz) CPU, 16 GB RAM, and an NVIDIA GeForce RTX 3060 GPU. The algorithms are programmed by Python3.12 using PyTorch 2.1.

## 5.1 2D Stokes problem

Consider the Stokes problem defined on  $\Omega = (0, 2) \times (-0.5, 1.5)$ , for which the exact solution is given by

$$u = 1 - e^{\zeta x} \cos(2\pi y), \quad v = \frac{\zeta}{2\pi} e^{\zeta x} \sin(2\pi y), \quad p = \frac{1}{2} e^{2\zeta x},$$

where  $\zeta = \frac{1}{2\nu} - \sqrt{\frac{1}{4\nu^2} + 4\pi^2}$ .

In this test case, we select 2500( $50 \times 50$ ) interior and 200( $50 \times 4$ ) boundary uniform grid points as the training samples, while an additional 12321( $111 \times 111$ ) uniform grid points are chosen as test samples.

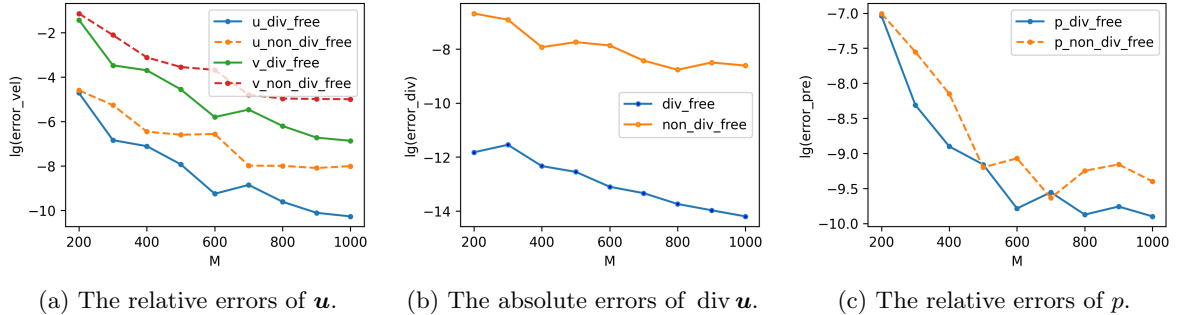


**Figure 5.1:** Numerical results for the 2D Stokes problem with  $\nu = 10^{-4}$  and varying numbers of basis functions.

We first compare the numerical performance of our proposed Decoupled-DFNN method with that of the standard TransNet. For a fixed kinematic viscosity  $\nu = 10^{-4}$ , Figure 5.1 shows the errors in velocity, divergence, and pressure with varying numbers of basis functions. The results indicate that Decoupled-DFNN not only achieves higher accuracy for velocity and pressure but also satisfies the incompressibility constraint more effectively, reaching a precision of at least  $\mathcal{O}(10^{-12})$ .

Moreover, Figure 5.2 demonstrates the superior efficiency of our method over the standard TransNet. While the computational cost of both approaches increases with the number of basis functions, the efficiency advantage of Decoupled-DFNN becomes more pronounced for larger basis sizes. This improvement is mainly due to the fact that the proposed method solves smaller and decoupled subproblems, rather than a large coupled system.

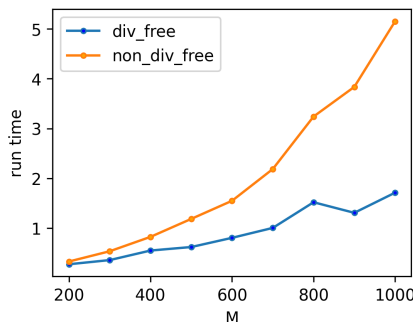


**Figure 5.2:** Execution time for the 2D Stokes problem with  $\nu = 10^{-4}$  across varying numbers of basis functions.

Next, we examine numerical performance across varying kinematic viscosity  $\nu$  with  $M =$

1000. As illustrated in Figure 5.3, Decoupled-DFNN demonstrates significantly superior performance in preserving the divergence-free condition. In terms of velocity accuracy, TransNet achieves slightly better results for larger viscosities, whereas Decoupled-DFNN performs significantly better for smaller viscosities ( $\nu \leq 10^{-2}$ ), outperforming TransNet by nearly two orders of magnitude. The pressure accuracy remains largely comparable between the two methods. This enhanced precision at lower viscosities underscores the robustness of the Decoupled-DFNN framework in high Reynolds-number regimes. Furthermore, variations in  $\nu$  have little effect on the computational cost. Overall, the execution time for Decoupled-DFNN is approximately 2 seconds, whereas the standard TransNet requires slightly over 5 seconds.

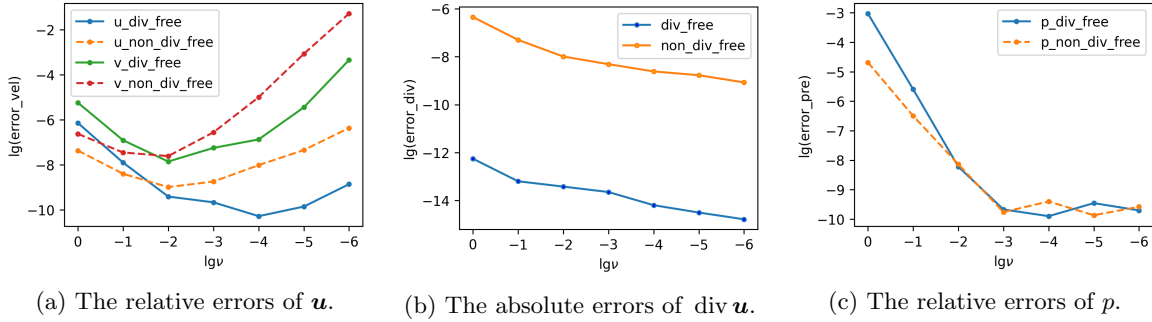


**Figure 5.3:** Numerical results for the 2D Stokes problem with  $M = 1000$  and varying kinematic viscosity.

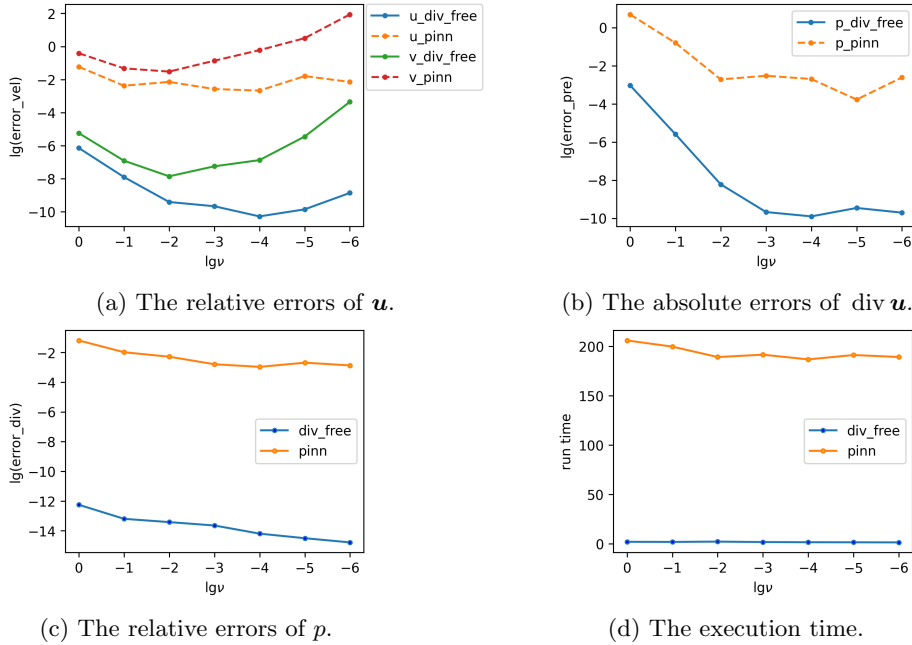


**Figure 5.4:** Numerical results of Decoupled-DFNN and PINN for the 2D Stokes problem.

Finally, we compare the performance of the proposed Decoupled-DFNN with PINN. For the PINN baseline, we employ 512 interior points and 256 boundary points and train the model for 10000 iterations. As shown in Figure 5.4, Decoupled-DFNN exhibits a clear advantage over PINN in both accuracy and computational efficiency. In particular, for velocity and pressure predictions, Decoupled-DFNN achieves errors that are at least four orders of magnitude smaller

than those of PINN. Notably, in low-viscosity regimes, PINN suffers from a complete loss of numerical accuracy, whereas the proposed method remains stable and accurate. In terms of enforcing physical constraints, Decoupled-DFNN achieves a relative divergence error on the order of  $\mathcal{O}(10^{-12})$ . By contrast, PINN, which imposes incompressibility through a penalty term in the loss function, attain divergence errors of only  $\mathcal{O}(10^{-3})$ . Moreover, Decoupled-DFNN solves the resulting linear least-squares problem in approximately 2 seconds, while PINNs require about 180 seconds to converge due to the non-convex and nonlinear nature of their optimization problem.

## 5.2 2D Navier-Stokes problem

Consider the Navier-Stokes problem defined on  $\Omega = (0, 1)^2$ , with the exact solution

$$u = 16y(y - 1)(2y - 1) \sin^2(\pi x), \quad v = -8\pi y^2(y - 1)^2 \sin(2\pi x), \quad p = \sin(\pi x) \cos(\pi y).$$

We employ the same training and test sets as those in subsection 5.1. Since the Gauss–Newton method is locally convergent, the PINN approximation obtained after 10000 training iterations is used as the initial guess. The maximum number of Gauss–Newton iterations is set to 40.

The numerical performance for  $M = 1000$  across varying kinematic viscosity  $\nu$  is showed in Figure 5.5. We observe that for  $\nu \leq 10^{-2}$ , TransNet and Decoupled-DFNN achieve comparable accuracy in both the velocity and pressure fields. This agreement in accuracy is expected, as both methods adopt the same initial guess and employ Newton-type iterations to solve the underlying nonlinear system. However, Decoupled-DFNN reduces the computational cost by more than 60%. This efficiency gain arises from the decoupled formulation, which involves solving significantly smaller-scale linear systems during each iteration compared to the fully coupled approach. Furthermore, Decoupled-DFNN maintains superior performance in strictly preserving the divergence-free constraint.

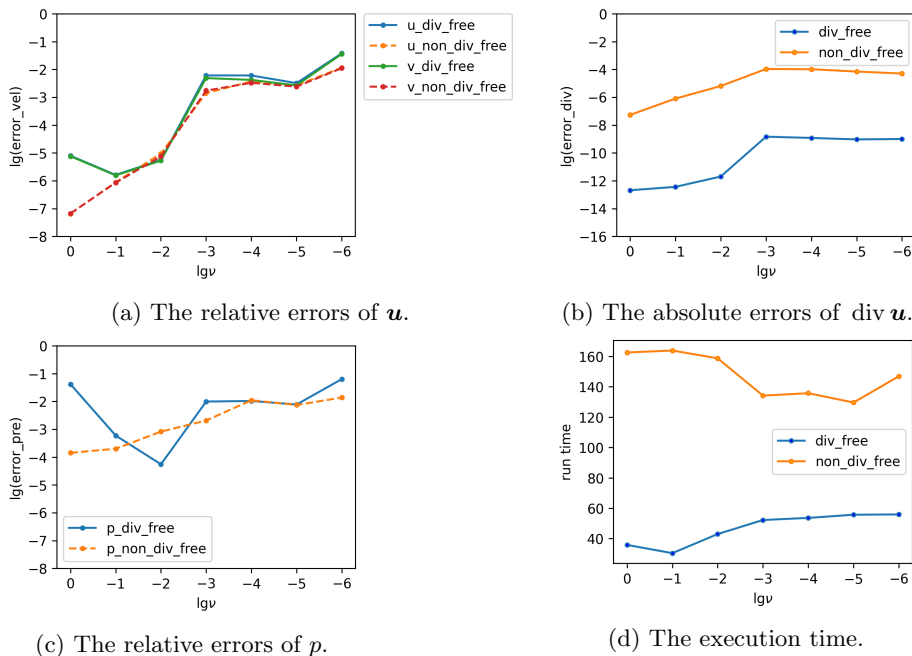


**Figure 5.5:** Numerical results for the 2D Navier-Stokes problem with  $M = 1000$  and varying  $\nu$ .

### 5.3 3D Stokes problem

Consider the Stokes problem defined on  $\Omega = (0, 1)^3$ , for which the analytical solution is given by

$$\begin{aligned} u &= e^{\cos(\pi y)} \sin(\pi z), & v &= e^{\cos(\pi z)} \sin(\pi x), & w &= e^{\cos(\pi x)} \sin(\pi y), \\ p &= e^{\cos(\pi x) + \sin(\pi y)} + e^{\cos(\pi z) + \sin(\pi x)}. \end{aligned}$$

For three-dimensional cases, we employ a Halton sampling strategy [3] to select 10000 interior points and 2400 boundary points (distributed as  $20 \times 20 \times 6$  uniform grids) for the training set. Additionally, 2000 interior Halton samples are chosen as the test set.

Consistent with the 2D results, we first compare the numerical results of Decoupled-DFNN and TransNet using varying numbers of basis functions, as shown in Figure 5.6. We observe that the approximate velocity field of Decoupled-DFNN is more accurate than that of TransNet for all values of  $M$ . While TransNet outperforms Decoupled-DFNN in pressure accuracy by approximately one order of magnitude when  $M$  is large, its execution time is nearly twice as long. Furthermore, the Decoupled-DFNN exhibits a significant advantage in its structure-preserving capability, surpassing TransNet by six orders of magnitude. With a divergence error of only  $10^{-14}$ , the incompressibility condition is satisfied almost exactly.

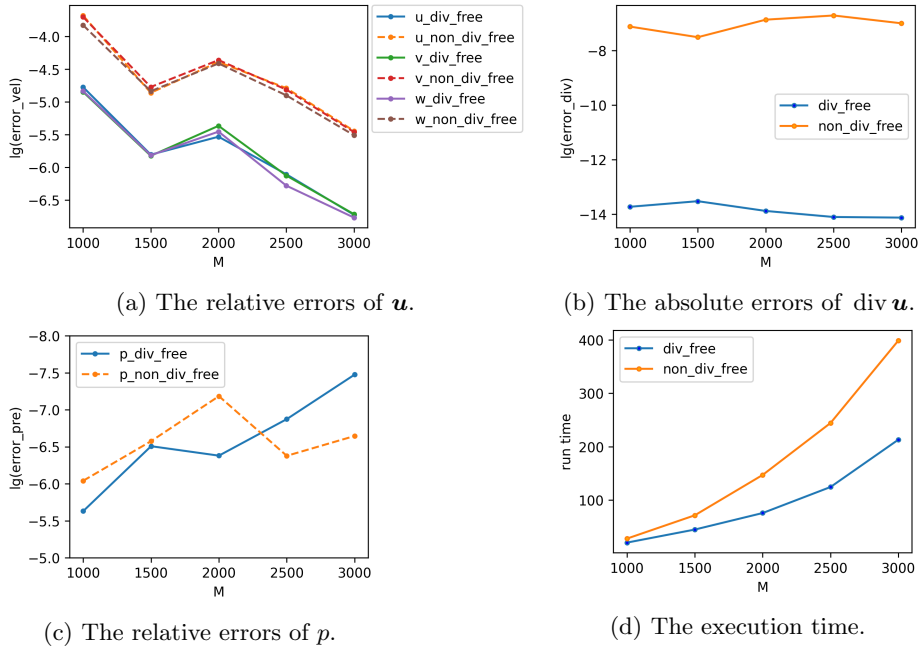


**Figure 5.6:** Numerical results for the 3D Stokes problem with  $\nu = 10^{-5}$  and varying  $M$ .

Next, we investigate the numerical robustness with respect to the viscosity coefficient  $\nu$  for both Decoupled-DFNN and TransNet, using a fixed  $M = 2500$  as shown in Figure 5.7. We find that the velocity error for Decoupled-DFNN initially decreases and subsequently increases as  $\nu$  is reduced, whereas the error for TransNet increases monotonically as  $\nu$  decreases. Therefore, Decoupled-DFNN demonstrates superior velocity accuracy in the low-viscosity regime ( $\nu \leq 10^{-4}$ ). Regarding pressure, the errors for both methods decrease as  $\nu$  is reduced, with Decoupled-DFNN outperforming TransNet specifically when  $\nu \leq 10^{-3}$ . Furthermore, the divergence-free condition in Decoupled-DFNN reaches machine precision, providing a significant advantage over TransNet across all values of  $\nu$ . Notably, the computational cost of Decoupled-DFNN is only half that of TransNet.

Finally, we demonstrate the advantages of Decoupled-DFNN over the standard PINN in Figure 5.8. The results indicate that Decoupled-DFNN achieves superior performance across all evaluated metrics, including velocity and pressure accuracy, adherence to the incompressibility condition, and computational efficiency.

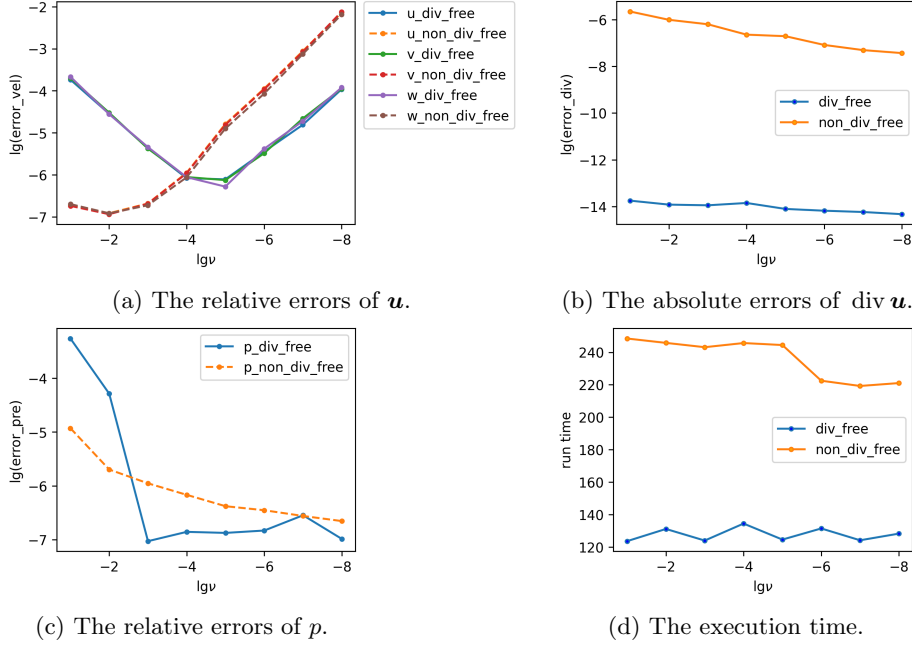


Figure 5.7: Numerical results for the 3D Stokes problem with  $M = 1500$  and varying  $\nu$ .

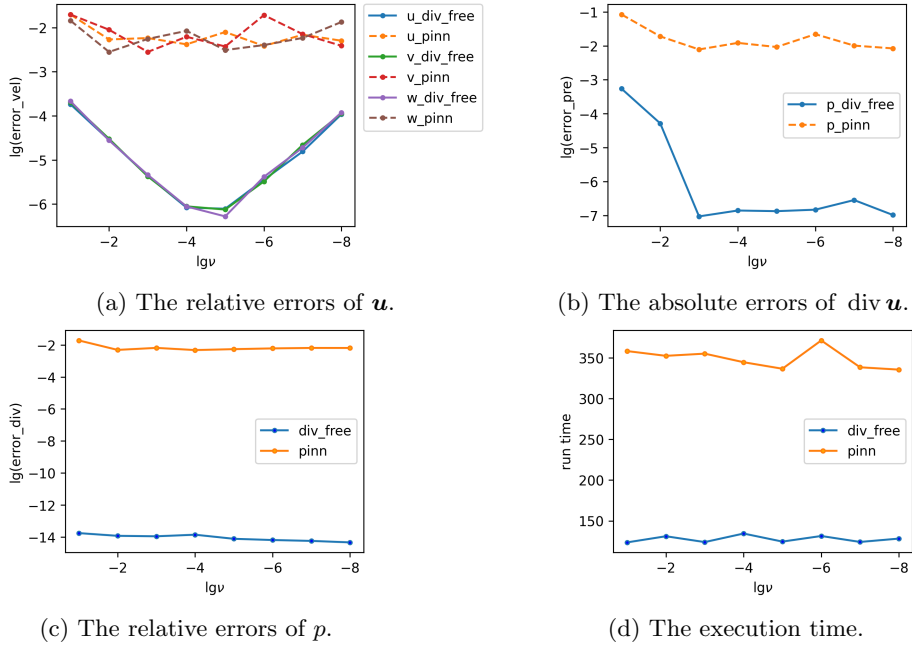


Figure 5.8: Numerical results of Decoupled-DFNN and PINN for the 3D Stokes problem.

## 5.4 3D Navier-Stokes problem

Consider the Navier-Stokes problem defined on  $\Omega = (0, 1)^3$ . The analytical solution reads

$$\begin{aligned} u &= 2(y-1)(z-1)\sin y \sin z - 2(y-1)\sin y \cos z - 2(z-1)\cos y \sin z, \\ v &= 2(z-1)(x-1)\sin z \sin x - 2(z-1)\sin z \cos x - 2(x-1)\cos z \sin x, \\ w &= 2(x-1)(y-1)\sin x \sin y - 2(x-1)\sin x \cos y - 2(y-1)\cos x \sin y, \\ p &= xyz + x^3y^3z - \frac{5}{32}. \end{aligned}$$

In this implementation, we employ the Gauss-Newton method to solve the resulting nonlinear systems. To accelerate convergence, the initial guess is taken from the approximation produced by Scheme I after 10 iterations (see the Appendix for details). The maximum number of iterations for the Gauss-Newton solver is set to 15.

Figure 5.9 shows the numerical performance of Decoupled-DFNN and TransNet for varying values of  $\nu$ . The results demonstrate that Decoupled-DFNN not only achieves higher accuracy in both velocity and pressure when  $\nu < 10^{-3}$ , but also maintains a significant advantage in enforcing the incompressibility constraint and reducing computational cost. These findings suggest that Decoupled-DFNN provides a more robust and efficient solution, particularly as the viscosity decreases and the flow becomes more challenging to resolve.

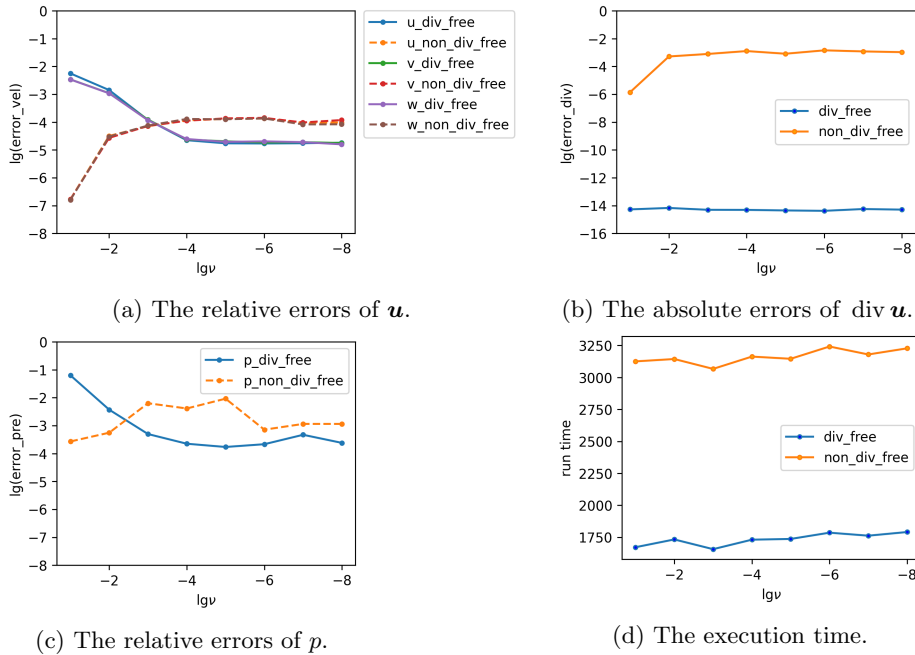


**Figure 5.9:** Numerical results for the 3D Stokes problem with  $M = 1500$  and varying  $\nu$ .

## 6 Conclusion

In this work, we present a decoupled divergence-free neural network method for solving incompressible flow problems, including the Stokes and Navier-Stokes problems. To ensure physical consistency, we adopt the stream function formulation in two-dimensions and vorticity-vector potential formulations in three-dimensions, and further exploit the properties of curl operator to derive fully decoupled divergence-free formulations about velocity and pressure. These formulation leads to a sequential solution strategy: the velocity field is first computed without in-

volution of the pressure, and the pressure field is then recovered. These decoupled subproblems are solved using the TransNet framework. To address the inherent nonlinearity of the Navier-Stokes equations, we further employ the Gauss-Newton method to linearize the governing equations, thereby transforming the problem into a sequence of linear subproblems. Numerical experiments demonstrate several key advantages of the Decoupled-DFNN:

- **Exact incompressibility:** The incompressibility constraint is satisfied up to nearly machine precision ( $10^{-14}$ ), significantly outperforming standard PINNs and TransNets that enforce this condition via soft penalty terms.
- **High efficiency:** The proposed method exhibits substantially reduced computational cost, requiring approximately 50% less execution time than comparable frameworks such as TransNet when using a large number of basis functions.
- **Enhanced stability:** The method achieves superior accuracy in velocity reconstruction, particularly in low-viscosity (high-Reynolds-number) regimes.

Overall, the proposed method offers a favorable balance between structure preservation and computational efficiency: it enforces the divergence-free condition exactly and reduces the complexity of the coupled system through decoupling, at the cost of higher regularity requirements, which are well accommodated by neural network approximations. Finally, we observe that the performance for the Stokes problem is generally better than that for the Navier-Stokes equations. One possible reason is the quality of the initial guess in the Gauss-Newton iteration. Improving the initialization strategy to enhance accuracy will be investigated in future work.

## Declarations

- **Code availability.** The codes during the current study are available from the corresponding author on reasonable request.
- **Authors' contributions.** All authors contributed equally to this manuscript.

## Acknowledgments

J. Huang and H. Wang were partially supported by NSFC (Grant No. 12571390). T. Zhou was supported by National Natural Science Foundation of China under grants 12288201 and 12461160275, and the Science challenge project No. TZ2025006.

## Appendix: Linearized Iterative Schemes

For completeness, we provide the specific formulations for the linearized iterative schemes, which serve as the initialization or alternative approaches to the Gauss-Newton iteration. Following the methodology in [41], the iterations for the velocity field in the 2D case (3.4) are defined as follows:

- Scheme I:

$$\nu \Delta^2 \phi^{(k+1)} - \operatorname{curl} \phi^{(k)} \cdot \nabla \Delta \phi^{(k+1)} = \mathbf{curl} \mathbf{f};$$

- Scheme II:

$$\nu \Delta^2 \phi^{(k+1)} - \operatorname{curl} \phi^{(k+1)} \cdot \nabla \Delta \phi^{(k)} = \mathbf{curl} \mathbf{f};$$

- Scheme III:

$$\nu \Delta^2 \phi^{(k+1)} - \frac{1}{2} (\operatorname{curl} \phi^{(k)} \cdot \nabla \Delta \phi^{(k+1)} + \operatorname{curl} \phi^{(k+1)} \cdot \nabla \Delta \phi^{(k)}) \operatorname{curl} \phi^{(k)} \cdot \nabla \Delta \phi^{(k+1)} = \mathbf{curl} \mathbf{f}.$$

Similarly, for the 3D case in (3.8), the corresponding schemes are given by:

- Scheme I:

$$\nu \Delta^2 \phi^{(k+1)} + (\Delta \phi^{(k+1)} \cdot \nabla) \operatorname{curl} \phi^{(k)} - (\operatorname{curl} \phi^{(k)} \cdot \nabla) \Delta \phi^{(k+1)} = \mathbf{curl} \mathbf{f};$$

- Scheme II:

$$\nu \Delta^2 \phi^{(k+1)} + (\Delta \phi^{(k)} \cdot \nabla) \operatorname{curl} \phi^{(k+1)} - (\operatorname{curl} \phi^{(k+1)} \cdot \nabla) \Delta \phi^{(k)} = \mathbf{curl} \mathbf{f};$$

- Scheme III:

$$\begin{aligned} \nu \Delta^2 \phi^{(k+1)} + \frac{1}{2} ((\Delta \phi^{(k+1)} \cdot \nabla) \operatorname{curl} \phi^{(k)} - (\operatorname{curl} \phi^{(k)} \cdot \nabla) \Delta \phi^{(k+1)} \\ + (\Delta \phi^{(k)} \cdot \nabla) \operatorname{curl} \phi^{(k+1)} - (\operatorname{curl} \phi^{(k+1)} \cdot \nabla) \Delta \phi^{(k)}) = \mathbf{curl} \mathbf{f}. \end{aligned}$$

## References

- [1] R. A. Adams, *Sobolev spaces*, Academic Press, New York-London, 1975.
- [2] A. R. Barron, *Universal approximation bounds for superpositions of a sigmoidal function*, IEEE Trans. Inform. Theory **39** (1993), no. 3, 930–945.
- [3] R. E. Caflisch, *Monte carlo and quasi-monte carlo methods*, Acta Numer. **7** (1998), 1–49.
- [4] W. Cai, S. Fang, and T. Zhou, *SOC-MartNet: a martingale neural network for the Hamilton-Jacobi-Bellman equation without explicit  $\inf_{u \in U} H$  in stochastic optimal controls*, SIAM J. Sci. Comput. **47** (2025), no. 4, C795–C819.
- [5] W. Cai, A. He, and D. Margolis, *DeepMartNet: A Martingale-Based Deep Neural Network Learning Method for Dirichlet BVPs and Eigenvalue Problems of Elliptic PDEs in  $\mathbb{R}^{d^*}$* , SIAM J. Sci. Comput. **48** (2026), no. 1, C25–C50.
- [6] F. Calabrò, G. Fabiani, and C. Siettos, *Extreme learning machine collocation for the numerical solution of elliptic PDEs with sharp gradients*, Comput. Methods Appl. Mech. Engrg. **387** (2021), Paper No. 114188, 17.
- [7] C. Canuto, M. Y. Hussaini, A. Quarteroni, and T. A. Zang, *Spectral Methods in Fluid Dynamics*, Springer, New York, 1988.
- [8] K.-C. Chang, *Methods in Nonlinear Analysis*, Springer-Verlag, Berlin, 2005.
- [9] F. Chen, J. Huang, C. Wang, and H. Yang, *Friedrichs learning: weak solutions of partial differential equations via deep learning*, SIAM J. Sci. Comput. **45** (2023), no. 3, A1271–A1299.
- [10] J. Chen, X. Chi, W. E, and Z. Yang, *Bridging traditional and machine learning-based algorithms for solving pdes: the random feature method*, J. Mach. Learn. **1** (2022), 268–298.
- [11] V. Cherepanov and S. W. Ertel, *Implicit deep random vortex methods for simulating incompressible flows in wall bounded domains*, Phys. Fluids **37** (2025), no. 3, 033118.
- [12] S. Cuomo, V. Schiano Di Cola, F. Giampaolo, and et al., *Scientific machine learning through physics-informed neural networks: where we are and what's next*, J. Sci. Comput. **92** (2022), no. 3, Paper No. 88, 62.
- [13] T. De Ryck, A. D. Jagtap, and S. Mishra, *Error estimates for physics-informed neural networks approximating the Navier-Stokes equations*, IMA J. Numer. Anal. **44** (2024), no. 1, 83–119.
- [14] T. De Ryck and S. Mishra, *Numerical analysis of physics-informed neural networks and related models in physics-informed machine learning*, Acta Numer. **33** (2024), 633–713.
- [15] R. DeVore, B. Hanin, and G. Petrova, *Neural network approximation*, Acta Numer. **30** (2021), 327–444.

- [16] S. Dong and Z. Li, *Local extreme learning machines and domain decomposition for solving linear and non-linear partial differential equations*, *Comput. Methods Appl. Mech. Engrg.* **387** (2021), Paper No. 114129, 63.
- [17] ———, *A modified batch intrinsic plasticity method for pre-training the random coefficients of extreme learning machines*, *J. Comput. Phys.* **445** (2021), Paper No. 110585, 31.
- [18] S. Dong and J. Yang, *On computing the hyperparameter of extreme learning machines: algorithm and application to computational PDEs, and comparison with classical and high-order finite elements*, *J. Comput. Phys.* **463** (2022), Paper No. 111290, 41.
- [19] Y. Du and T. A. Zaki, *Evolutional deep neural network*, *Phys. Rev. E* **104** (2021), no. 4, Paper No. 045303, 14.
- [20] V. Dwivedi and B. Srinivasan, *Physics informed extreme learning machine (PIELM)—a rapid method for the numerical solution of partial differential equations*, *Neurocomputing* **391** (2020), 96–118.
- [21] W. E, *Machine learning and computational mathematics*, *Commun. Comput. Phys.* **28** (2020), no. 5, 1639–1670.
- [22] W. E, J. Han, and A. Jentzen, *Deep learning-based numerical methods for high-dimensional parabolic partial differential equations and backward stochastic differential equations*, *Commun. Math. Stat.* **5** (2017), no. 4, 349–380.
- [23] ———, *Algorithms for solving high dimensional PDEs: from nonlinear Monte Carlo to machine learning*, *Nonlinearity* **35** (2022), no. 1, 278–310.
- [24] W. E and J.-G. Liu, *Finite difference methods for 3D viscous incompressible flows in the vorticity-vector potential formulation on nonstaggered grids*, *J. Comput. Phys.* **138** (1997), no. 1, 57–82.
- [25] W. E and B. Yu, *The deep Ritz method: a deep learning-based numerical algorithm for solving variational problems.*, *Commun. Math. Stat.* **6** (2018), 1–12.
- [26] V. Girault and P.-A. Raviart, *Finite Element Methods for Navier-Stokes Equations*, Springer, Berlin, 1986.
- [27] B.-Y. Guo and He L.-P., *The fully discrete Legendre spectral approximation of two-dimensional unsteady incompressible fluid flow in stream function form*, *SIAM J. Numer. Anal.* **35** (1998), no. 1, 146–176.
- [28] B.-Y. Guo, He L.-P., and D.-K. Mao, *On the two-dimensional Navier-Stokes equations in stream function form*, *J. Math. Anal. Appl.* **205** (1997), no. 1, 1–31.
- [29] K. He, X. Zhang, S. Ren, and J. Sun, *Deep residual learning for image recognition*, 2016 IEEE Conference on Computer Vision and Pattern Recognition, 2016.
- [30] K. Hornik, M. Stinchcombe, and H. White, *Multilayer feedforward networks are universal approximators*, *Neural Netw.* **2** (1989), no. 5, 359 – 366.
- [31] G.-B. Huang, Q.-Y. Zhu, and C.-K. Siew, *Extreme learning machine: Theory and applications*, *Neurocomputing* **70** (2006), no. 1, 489–501.
- [32] J. Huang and H. Wu, *The neural network basis method for nonlinear partial differential equations and its Gauss-Newton optimizer*, *Commun. Nonlinear Sci. Numer. Simul.* **143** (2025), Paper No. 108608, 19.
- [33] J. Huang, H. Wu, and T. Zhou, *Adaptive neural network basis methods for partial differential equations with low-regular solutions*, *Commun. Comput. Phys.* **39** (2026), no. 2, 553–577.
- [34] C. Huré, H. Pham, and X. Warin, *Deep backward schemes for high-dimensional nonlinear PDEs*, *Math. Comp.* **89** (2020), no. 324, 1547–1579.
- [35] X. Jin, S. Cai, H. Li, and G. E Karniadakis, *NSFnets (Navier-Stokes flow nets): physics-informed neural networks for the incompressible Navier-Stokes equations*, *J. Comput. Phys.* **426** (2021), Paper No. 109951, 26.
- [36] G.E. Karniadakis, I.G. Kevrekidis, L. Lu, et al., *Physics-informed machine learning*, *Nat Rev Phys.* **3** (2021), 422–440.
- [37] A. Kashfi and T. Mukerji, *Physics-informed PointNet: a deep learning solver for steady-state incompressible flows and thermal fields on multiple sets of irregular geometries*, *J. Comput. Phys.* **468** (2022), Paper No. 111510, 31.
- [38] D. P. Kingma and J. Ba, *Adam: a method for stochastic optimization*, The 3rd International Conference on Learning Representations, 2015.
- [39] J. Lequeurre and A. Munnier, *Vorticity and stream function formulations for the 2D Navier-Stokes equations in a bounded domain*, *J. Math. Fluid Mech.* **22** (2020), no. 2, Paper No. 15, 73.

- [40] J.-G. Liu and W. E, *Simple finite element method in vorticity formulation for incompressible flows*, Math. Comp. **70** (2001), no. 234, 579–593.
- [41] L. Liu, B. Wang, and W. Cai, *Linearized learning with multiscale deep neural networks for stationary Navier-Stokes equations with oscillatory solutions*, East Asian J. Appl. Math. **13** (2023), no. 3, 740–758.
- [42] Y. Liu and C. Yang, *VPVnet: a velocity-pressure-vorticity neural network method for the Stokes' equations under reduced regularity*, Commun. Comput. Phys. **31** (2022), no. 3, 739–770.
- [43] L. Lu, X. Meng, Z. Mao, and G. E. Karniadakis, *DeepXDE: a deep learning library for solving differential equations*, SIAM Rev. **63** (2021), no. 1, 208–228.
- [44] N. Margenberg, D. Hartmann, C. Lessig, and T. Richter, *A neural network multigrid solver for the Navier-Stokes equations*, J. Comput. Phys. **460** (2022), Paper No. 110983, 19.
- [45] N. Margenberg, R. Jendersie, C. Lessig, and T. Richter, *DNN-MG: a hybrid neural network/finite element method with applications to 3D simulations of the Navier-Stokes equations*, Comput. Methods Appl. Mech. Engrg. **420** (2024), Paper No. 116692, 30.
- [46] N. Margenberg, C. Lessig, and T. Richter, *Structure preservation for the deep neural network multigrid solver*, Electron. Trans. Numer. Anal. **56** (2022), 86–101.
- [47] P. Minakowski and T. Richter, *A priori and a posteriori error estimates for the Deep Ritz method applied to the Laplace and Stokes problem*, J. Comput. Appl. Math. **421** (2023), Paper No. 114845, 16.
- [48] L. Quartapelle, *Numerical Solution of the Incompressible Navier-Stokes Equations*, Birkhäuser Verlag, Basel, 1993.
- [49] A. Quarteroni and A. Valli, *Numerical Approximation of Partial Differential Equations*, Springer, Berlin, 1994.
- [50] M. Raissi, P. Perdikaris, and G. E. Karniadakis, *Physics-informed neural networks: a deep learning framework for solving forward and inverse problems involving nonlinear partial differential equations*, J. Comput. Phys. **378** (2019), 686–707.
- [51] Y. Shang, F. Wang, and J. Sun, *Randomized neural network with Petrov-Galerkin methods for solving linear and nonlinear partial differential equations*, Commun. Nonlinear Sci. Numer. Simul. **127** (2023), Paper No. 107518, 20.
- [52] H. Sun, M. Hou, Y. Yang, and et al., *Solving partial differential equation based on Bernstein neural network and extreme learning machine algorithm*, Neural Process Lett. **50** (2019), 1153–1172.
- [53] J. Sun, S. Dong, and F. Wang, *Local randomized neural networks with discontinuous Galerkin methods for partial differential equations*, J. Comput. Appl. Math. **445** (2024), Paper No. 115830, 25.
- [54] R. Temam, *Navier-Stokes Equations*, revised ed., North-Holland Publishing Co., Amsterdam-New York, 1979.
- [55] M. Weng, Z. Mao, and J. Shen, *Deep collocation method: A framework for solving PDEs using neural networks with error control*, SIAM J. Sci. Comput. **48** (2026), no. 1, C77–C102.
- [56] Y. Zang, G. Bao, X. Ye, and H. Zhou, *Weak adversarial networks for high-dimensional partial differential equations*, J. Comput. Phys. **411** (2020), Paper No. 109409, 14.
- [57] R. Zhang, P. Hu, Q. Meng, and et al, *DRVN (deep random vortex network): A new physics-informed machine learning method for simulating and inferring incompressible fluid flows*, Phys. Fluids **34** (2022), no. 10, Paper No. 107112, 21.
- [58] Z. Zhang, F. Bao, L. Ju, and G. Zhang, *Transferable neural networks for partial differential equations*, J. Sci. Comput. **99** (2024), no. 1, Paper No. 2, 25.